



On wave propagation of rotating viscoelastic nanobeams with temperature effects by using modified couple stress-based nonlocal Eringen's theory

Arash Rahmani¹ · Babak Safaei^{2,4} · Zhaoye Qin³

Received: 15 December 2020 / Accepted: 17 May 2021 / Published online: 24 May 2021
© The Author(s), under exclusive licence to Springer-Verlag London Ltd., part of Springer Nature 2021

Abstract

In the current research, a comprehensive wave propagation analysis is performed on rotating viscoelastic nanobeams resting on Winkler-Pasternak foundations under thermal effects. Here, a novel non-classical mechanical model is developed to describe accurate wave propagation behavior for viscoelastic nanobeams. Employing nonlocal Eringen's theory along with modified couple stress theory, our proposed model, for the first time, simultaneously takes into account particle interactions and size dependency effects in nanobeams during wave propagation. To capture both hardening and softening behaviors of materials during wave propagation, nonlocal Eringen's theory and modified couple stress theories are merged. As a higher-order shear deformation theory, Reddy's beam theory (RBT) is adopted to develop motion equations for nanobeams, which are then analytically solved to obtain numerical results. The results are illustrated for all torsional (TO), transverse (TA) and longitudinal (LA) wave propagation patterns are comprehensively discussed in detail. Finally, the effects of nonlocal parameter to length scale ratios, Winkler-Pasternak coefficients, thermal gradient, slenderness ratios and rotating velocity of viscoelastic nanobeam are investigated and discussed.

Keywords Wave propagation · Analytic solution · Rotating viscoelastic nanobeam · Temperature effects · Nonlocal modified couple stress theory

1 Introduction

Recently, micro/nano structures are increasingly applied because of their extraordinary electrical, thermal and mechanical properties [1–7]. Since micro/nano structures

emerge as the next-generation technology, which are capable of making a significant difference in people's lives and nanobeams are an important element of micro/nano structures, comprehensive studies such as these structures are necessary [8–14]. Some practical applications of micro/nano structures are: sensors, MEMS/NEMS devices, miniature robots, micro/nano tools, lens, and lasers [15, 16]. These devices have been applied in several industries such as aerospace, wireless networks, optical, biomedical, drug delivery systems and consumer products. Accordingly, accurate evaluation and detailed investigation of the mechanical behaviors of micro/nano structures including bending [17–19], buckling [10, 20], vibration [21–25] and wave propagation [26–30] are necessary to increase their reliability and obtain the proper design of small-scale systems. Due to the deficiency of classical continuum mechanics theories in analyzing the mechanical behaviors of micro/nano structures, modified elasticity theories such as couple stress (CS), strain gradient (SG), general nonlocal (GN) and Eringen's nonlocal (EN) theories [4, 31–36] have been proposed to resolve these problems. Also, in the past 2 years, combined non-classical elasticity theories such as nonlocal strain gradient

✉ Arash Rahmani
arash.rahmani@uut.ac.ir

✉ Babak Safaei
babak.safaei@emu.edu.tr

Zhaoye Qin
qinzy@mail.tsinghua.edu.cn

¹ Department of Mechanical Engineering, Urmia University of Technology, Urmia, Iran

² Department of Mechanical Engineering, Eastern Mediterranean University, Famagusta, North Cyprus via Mersin 10, Turkey

³ Department of Mechanical Engineering, Tsinghua University, Beijing 100084, China

⁴ Department of Mechanical Engineering Science, University of Johannesburg, Gauteng 2006, South Africa

(NL-SG) theory have attracted the interests of researchers [37–40]. Ebrahimi et al. [41] investigated the wave propagation-thermal behaviors of graphene nanoplatelet-reinforced composite (GNPRC) porous cylindrical nanoshells on the basis of nonlocal strain gradient theory (NSGT) taking into account the calibrated values of nonlocal constant and material length scale parameter. Al-Furjan et al. [42] performed wave propagation simulations on multi-hybrid nanocomposite (MHC) reinforced doubly curved panels covered with piezoelectric actuators to reveal the effects of electrical load on the wave responses of smart panels. Zenkour and Sobhy [43] studied size-dependent wave propagation in functionally graded (FG) graphene platelet (GPL)-reinforced composite bi-layer nanobeams embedded in Pasternak elastic foundation.

Many researchers have considered the mechanical behaviors of micro/nano structures in recent years. The following literature review is allocated to the investigation of wave propagation behaviors of such small-scale elements. Kocaturk and Akbas [44] employed Bernoulli–Euler beam model and modified couple stress theory (MCST) to investigate the wave propagation behavior of nanobeams. Lim et al. [45] proposed a higher-order model capable of coupling nonlocal stresses and strain gradients to analyze wave propagation. They considered Timoshenko and Euler–Bernoulli nanobeams as examples and performed comprehensive tests. Li et al. [46] used Euler–Bernoulli beam model and nonlocal SG theory to study wave propagation in FG nanobeams. Ma et al. [47] illustrated wave propagation of smart nanobeam structures on the basis of nonlocal Timoshenko beam theory. Arefi and Zenkour [48] studied wave propagation in smart Timoshenko FG nanobeams via nonlocal elasticity theory. Barati and Zenkour [49] studied wave propagations in porous nanobeams establishing a general bi-Helmholtz NL-SG model. Narendar and Gopalakrishnan [50] investigated wave propagation performance in a rotating nanotube on the basis of EN theory. In another work, Sobhi and Zenkour [51] studied the bending of viscoelastic nanobeams laying on visco-Pasternak elastic foundations on the basis of a new shear and normal deformations beam theory. Zenkour et al. [52] showed that damping time and deflection were inversely proportional to thickness ratio, modes, thickness and aspect ratio of magnetostrictive layer to viscoelastic layer. In another work, Zenkour and El-Shahrany [53] investigated the vibration behaviors of magnetostrictive laminated beams resting on visco-Pasternak foundation.

Ebrahimi and Haghi [54] reported wave propagations in rotating FG nanoscale-beams by taking thermal effects into account on the basis of NL-SG theory. Moreover, they investigated the effect of fiber angle on the wave propagation behaviors of laminated cylindrical micro-shells. Zeighampour and Tadi Bani [55] performed wave desperation in FG-CNTRC cylindrical micro-shells considering NL-SG and

shear deformable shell theory. Ebrahimi and Dabbagh [56] studied wave propagation behaviors of piezoelectric nanoplates on elastic foundations. They employed NL-SG and Kirchhoff plate theories for model development. They also considered surface effects in extracting results. Shahsavari et al. [57] studied wave propagations in FG nano-plates on hybrid foundations considering thermal effects. They applied bi-Helmholtz NL-SG along with refined-higher order shear deformation plate theory for model establishing. Barati [58] studied wave propagation in bonded nanobeams with imperfections. He used general NL-SG model and refined shear deformation beam theory for the investigation of the effects of porosity and temperature on wave dispersion. Liu and Lv [59] investigated the effects of uncertain material properties on the wave propagations of smart nanobeams on the basis of nonlocal theory and Euler–Bernoulli beam model. Amiri et al. [60] employed NL-SG theory for the evaluation of wave propagation of smart piezoelectric nanotubes conveying viscous fluids. They took into account slip boundary conditions and surface stress effects. Ma et al. [61] reported wave dispersion behaviors of piezoelectric nano-plates on the basis of the NL theory and Kirchhoff and Mindlin nano-plate models considering thermo-electro-mechanical loads. Karami et al. [62] utilized NL-SG theory to evaluate hydrothermal wave propagation in viscoelastic graphene and nano-plate porous heterogeneous materials exposed to magnetic fields. She et al. [63] employed NL-SG theory to analyze the wave propagations of nano-tube wave propagations. More recently, She et al. [64] employed NL-SG theory and Reddy's high order beam model to explore wave propagations in FG porous nanobeams. Zeighampour et al. [65] studied the wave propagation behaviors of viscoelastic nanotubes according to NL-SG and shell theories. Sobhy and Zenkour [51] applied normal and shear deformations beam theory to investigate the static and dynamic bendings of viscoelastic nanobeams resting on visco-Pasternak elastic foundations.

Recently, Ebrahimi and Dabbagh [66] performed detailed investigations on wave propagation in FG porous nano-structures. They took into account coupling effects between Young's moduli and density in porous materials. Masoumi et al. [67] explored the wave propagations of piezoelectric nanobeams using NL-SG theory and Reddy's beam model to derive their governing equations and harmonic wave dispersion. Karami and Janghorban [68] reported transverse and longitudinal wave desperations of triclinic nanobeams for the first time on the basis of NL-SG and size-dependent shear deformation theories considering stretching effect. Wang and Liang [69] studied wave dispersion behaviors of nanobeams made of nano-porous metal foams using nonlocal elasticity theory and Timoshenko and Euler–Bernoulli beam models. Sobhy and Zenkour [70] utilized NL-SG theory to investigate wave propagations in bi-layer porous FG

nano-plates in Winkler elastic medium. Also, Abouelregal and Zenkour [71] studied the vibrations of viscoelastic FG Euler–Bernoulli nanostructure beams using fractional-order calculus. Arani et al. [72] used NL theory considering surface and flexoelectric effects to illustrate wave propagations in FG nanobeams resting on elastic media. They extracted motion governing equations on the basis of Timoshenko beam model with residual surface stress. Ebrahimi et al. [41] used NL-SG theory for the analysis of wave propagation in graphene nano-platelet-reinforced composite porous cylindrical nano-shells considering thermal effects. Cao and Wang [73] employed NL-SG Rayleigh beam theory for the evaluation of wave propagations in viscoelastic lipid nanotubes conveying protein. Faroughi et al. [74] studied wave propagations in bi-directional FG rotating nanobeams based on GN theory and higher-order Reddy’s beam model. Recently, to more accurately capture size effects, some researchers have proposed the consolidation of non-classical theories for the analysis of micro/nano structures [75, 76]. Hence, in the current work, we have tried to present different possibilities of coupling effects of nonlocal elasticity and modified couple stress theories, so-called nonlocal modified couple stress theory (NL-MCST), for rotating nanobeams resting on visco-elastic foundations. We employed NL-MCST to capture the effect of the rotational degree of freedom of particles as well as nonlocal and long-range interactions between particles simultaneously. We propose to study the accuracy of our model in comparison to other models. Some other investigations have considered the coupling effects of modified couple stress and Eringen’s nonlocal theories simultaneously [77, 78]. Ebrahimi and Barati [79] performed vibration analyses on FG nanobeams using nonlocal elasticity and modified couple stress theories. They also applied Galerkin’s method to obtain numerical results. Shariati et al. [80] presented the vibrational characteristics of FG nanobeams via the combination of nonlocal and couple stress theories considering surface effects. Ramezani and Mojra [81] conducted stability analyses on carbon nanotubes conveying nano-fluid under magnetic field. They used nonlocal elasticity and couple stress theories to construct a model and coupled Euler–Bernoulli beam theory with Navier–Stokes’s equation of magnetic-fluid flow to determine fluid–structure interactions. Attar et al. [82] investigated the vibrational behaviors of FG piezoelectric (FGP) plates considering simultaneous effects of nonlocal and couple stress based on Kirchhoff thin plate theory and Navier’s approach.

According to the above literature review, it was found that the existing reports on wave propagation in small-scale beams are mainly based on EN, SG, MCST and especially NL-SG theories. It is noteworthy that, unlike NL-SG theory, a clear gap in other studies is that the consolidation of Eringen’s nonlocal and modified couple stress theories has not

been considered for wave propagation analysis yet. Hence, in this study, the combined effects of modified couple stress and nonlocal Eringen’s theories are employed to indicate the effect of local rotational DOF. Then, this effect is expressed in the framework of ENT which covers long-range and non-local interactions among particles. To capture both softening and hardening behaviors of materials, modified couple stress and nonlocal Eringen’s theories are combined. Actually, we illustrated that the waiver of couple stress effect decreases frequencies by decreasing nanobeam stiffness. Also, waiver the effect of nonlocal parameter makes nanobeams stiffer, which increases frequencies. Hence, the wave frequency predicted by NL-MCST theory is always between the values obtained from ENT and MCST theories. Furthermore, as a higher-order shear deformation theory, RBT is adopted to establish an accurate model and corresponding analytic solutions are obtained as numerical results. The results are illustrated for all torsional (TO), transverse (TA) and longitudinal (LA) wave propagations and are comprehensively discussed. In addition to this novel consideration, the current comprehensive study encompasses the interactions of rotation, thermal and viscoelastic effects of higher-order-shear deformation beam model.

2 Formulation

2.1 Description

As shown in Fig. 1, a rotating viscoelastic nanobeam resting on a Winkler–Pasternak foundation is adopted to consider thermal effects. The nanobeam has length L , width b , rectangular cross-section a and thickness h .

2.2 Kinematics

Reddy’s beam theory, namely third-order shear deformation theory, is adopted to develop the kinematics model of viscoelastic nanobeams resting on Winkler–Pasternak foundations. Displacement fields are described as:

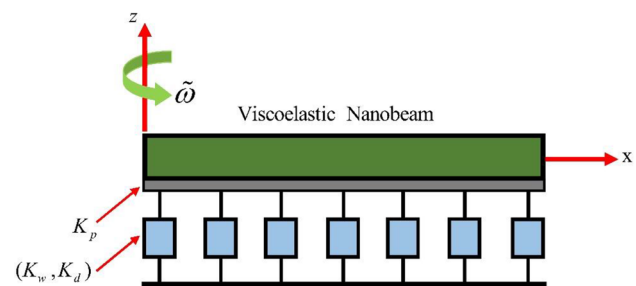


Fig. 1 Rotating viscoelastic nanobeam resting on a Winkler–Pasternak foundation

$$\mathbf{u} = (u_1, u_2, u_3), \tag{1}$$

$$u_1 = u + z\varphi - c_1 z^3 \left(\varphi + \frac{\partial w}{\partial x} \right); u_2 = 0; u_3 = w, \tag{2}$$

where w and u are transverse and longitudinal displacements, φ is the rotation of neutral axis cross-section and $c_1 = 4/(3h^2)$.

The strains of Reddy beam model are expressed as:

$$\varepsilon_{xx} = \frac{\partial u_1}{\partial x} = \frac{\partial u}{\partial x} + z \frac{\partial \varphi}{\partial x} - c_1 z^3 \left(\frac{\partial \varphi}{\partial x} + \frac{\partial^2 w}{\partial x^2} \right), \tag{3a}$$

$$2\varepsilon_{xz} = \frac{\partial u_1}{\partial z} + \frac{\partial u_3}{\partial x} = \left(\varphi + \frac{\partial w}{\partial x} \right) - c_2 z^2 \left(\varphi + \frac{\partial w}{\partial x} \right), \tag{3b}$$

where rotation vector $\boldsymbol{\theta}$ and symmetric curvature tensor χ_{ij} are given as:

$$\boldsymbol{\theta} = \frac{1}{2} \text{curl} \mathbf{u}, \tag{4}$$

$$\chi_{ij} = \frac{1}{2} (\theta_{i,j} + \theta_{j,i}). \tag{5}$$

Substitution of Eq. (5) in Eq. (4) yields:

$$2\chi_{yx} = \frac{1}{2} \left(\frac{\partial \varphi}{\partial x} - \frac{\partial^2 w}{\partial x^2} - c_2 z^2 \left(\frac{\partial \varphi}{\partial x} + \frac{\partial^2 w}{\partial x^2} \right) \right), \tag{6a}$$

$$2\chi_{yz} = -c_2 z \left(\varphi + \frac{\partial w}{\partial x} \right), \tag{6b}$$

where $c_2 = 3c_1$.

3 Modified couple stress theory

According to modified couple stress theory [34], strain energy density Π_s is given in terms of strain and curvature conjugated with stress and couple stress, respectively, as:

$$\Pi_s = \int_0^L \int_A (\boldsymbol{\sigma} : \boldsymbol{\varepsilon} + \mathbf{m} : \boldsymbol{\chi}) dA dx, \tag{7}$$

where $\boldsymbol{\sigma}$, $\boldsymbol{\varepsilon}$, $\boldsymbol{\chi}$ are stress, strain and curvature tensors, respectively and, \mathbf{m} is the deviatoric part of couple stress tensor and can be expressed as:

$$m_{ij} = 2G l_m^2 \chi_{ij}, \tag{8}$$

where G and l_m are shear modulus of rigidity and non-classical length scale parameter, respectively. By substituting Eqs. (3) and (6) into Eq. (7) and using some algebraic simplifications, strain energy density is obtained as:

$$\Pi_s = \int_0^L \left[\begin{aligned} &M_{xx}^{(0)} \frac{\partial u}{\partial x} + M_{xx}^{(1)} \frac{\partial \varphi}{\partial x} - c_1 M_{xx}^{(3)} \left(\frac{\partial \varphi}{\partial x} + \frac{\partial^2 w}{\partial x^2} \right) \\ &+ Q_{xz}^{(0)} \left(\varphi + \frac{\partial w}{\partial x} \right) - c_2 Q_{xz}^{(2)} \left(\varphi + \frac{\partial w}{\partial x} \right) \\ &+ \frac{1}{2} Y_{yx}^{(0)} \left(\frac{\partial \varphi}{\partial x} - \frac{\partial^2 w}{\partial x^2} \right) \\ &- \frac{c_2}{2} Y_{yx}^{(2)} \left(\frac{\partial \varphi}{\partial x} + \frac{\partial^2 w}{\partial x^2} \right) \\ &- c_2 Y_{yz}^{(1)} \left(\varphi + \frac{\partial w}{\partial x} \right) \end{aligned} \right] dx, \tag{9}$$

where:

$$\begin{aligned} M_{xx}^{(i)} &= \int_A \sigma_{xx} z^i dA; Q_{xz}^{(i)} = \int_A \sigma_{xz} z^i dA; Y_{yx}^{(i)} \\ &= \int_A m_{yx} z^i dA; Y_{yz}^{(i)} = \int_A m_{yz} z^i dA. \end{aligned} \tag{10}$$

4 Governing equations of motion

Based on Hamilton’s principle, motion equations can be defined as:

$$\delta H = \delta \int_{t_1}^{t_2} (\Pi_k - (\Pi_s + \Pi_w)) dt = 0, \tag{11}$$

where Π_k , Π_s and Π_w indicate kinetic energy, strain energy and the work done by external forces, respectively.

Kinetic energy Π_k is defined as:

$$\begin{aligned} \Pi_k &= \frac{1}{2} \rho \int_0^L \int_A \left(\left(\frac{\partial u_1}{\partial t} \right)^2 + \left(\frac{\partial u_2}{\partial t} \right)^2 + \left(\frac{\partial u_3}{\partial t} \right)^2 \right) dA dx \\ &= \frac{1}{2} \int_0^L \left[\begin{aligned} &m_0 \left(\frac{\partial u}{\partial t} \right)^2 + m_2 \left(\frac{\partial \varphi}{\partial t} \right)^2 \\ &+ c_1^2 m_6 \left(\frac{\partial \varphi}{\partial t} + \frac{\partial^2 w}{\partial x \partial t} \right)^2 \\ &+ 2m_1 \left(\frac{\partial u}{\partial t} \right) \left(\frac{\partial \varphi}{\partial t} \right) \\ &- 2c_1 m_3 \left(\frac{\partial u}{\partial t} \right) \left(\frac{\partial \varphi}{\partial t} + \frac{\partial^2 w}{\partial x \partial t} \right) \\ &- 2c_1 m_4 \left(\frac{\partial \varphi}{\partial t} \right) \left(\frac{\partial \varphi}{\partial t} \right. \\ &\left. + \frac{\partial^2 w}{\partial x \partial t} \right) + m_0 \left(\frac{\partial w}{\partial t} \right)^2 \end{aligned} \right] dx, \end{aligned} \tag{12}$$

where:

$$m_i = \int_A \rho z^i dA, \tag{13}$$

$$\bar{m}_i = m_i - c_1 m_{i+2} = \rho \bar{l}_i; \hat{m}_i = \bar{m}_i - c_1 \bar{m}_{i+2} = \rho \hat{l}_i. \tag{14}$$

Also, the first variations of Π_k, Π_s and Π_w are defined as the following:

$$\delta\Pi_k = \int_0^L \left[\left(-m_0 \frac{\partial^2 u}{\partial t^2} - \bar{m}_1 \frac{\partial^2 \varphi}{\partial t^2} + c_1 m_3 \frac{\partial^3 w}{\partial x \partial t^2} \right) \delta u - \left(\bar{m}_1 \frac{\partial^2 u}{\partial t^2} + \hat{m}_2 \frac{\partial^2 \varphi}{\partial t^2} - c_1 \bar{m}_4 \frac{\partial^3 w}{\partial x \partial t^2} \right) \delta \varphi - \left(m_0 \frac{\partial^2 w}{\partial t^2} + c_1 m_3 \frac{\partial^3 u}{\partial x \partial t^2} + c_1 \bar{m}_4 \frac{\partial^3 \varphi}{\partial x \partial t^2} - c_1^2 m_6 \frac{\partial^4 w}{\partial x^2 \partial t^2} \right) \delta w \right] dx, \tag{15}$$

$$\delta\Pi_s = \int_0^L \left[\left(-\frac{\partial M_{xx}^{(0)}}{\partial x} \right) \delta u - \left(\frac{\partial \bar{M}_{xz}^{(1)}}{\partial x} - \bar{Q}_{xz}^{(0)} + \frac{\partial \bar{Y}_{yx}^{(0)}}{\partial x} + c_2 Y_{yz}^{(1)} \right) \delta \varphi - \left(c_1 \frac{\partial^2 M_{xx}^{(3)}}{\partial x^2} + \frac{\partial \bar{Q}_{xz}^{(0)}}{\partial x} + \frac{\partial^2 \bar{Y}_{yx}^{(0)}}{\partial x^2} - c_2 \frac{\partial Y_{yz}^{(1)}}{\partial x} \right) \delta w \right] dx, \tag{16}$$

$$\delta\Pi_w = - \int_0^L \left[\left(-\frac{\partial}{\partial x} \left(N_T \frac{\partial w}{\partial x} \right) + q - K_w w - K_d \frac{\partial w}{\partial t} + K_p \frac{\partial^2 w}{\partial x^2} + \frac{\partial}{\partial x} \left(T(x) \frac{\partial w}{\partial x} \right) \right) \delta w + f \delta u \right] dx, \tag{17}$$

in which:

$$\bar{M}_{xx}^{(1)} = M_{xx}^{(1)} - c_1 M_{xx}^{(3)}; \bar{Q}_{xz}^{(0)} = Q_{xz}^{(0)} - c_2 Q_{xz}^{(2)}, \tag{18}$$

$$\bar{Y}_{yx}^{(0)} = \frac{1}{2} \left(Y_{yx}^{(0)} - c_2 Y_{yx}^{(2)} \right); \bar{Y}_{yx}^{(1)} = \frac{1}{2} \left(Y_{yx}^{(0)} + c_2 Y_{yx}^{(2)} \right), \tag{19}$$

$N_T = \int_A (E\alpha\Delta T)dA$ is applied axial thermal force, and q and f are transverse and longitudinal distributed forces, respectively. Also, K_w, K_d, K_p are Winkler, Pasternak and damping coefficients due to elastic foundation, respectively, and $T(x)$ is the axial force due to centrifugal stiffening resulting from nanobeam rotation given as:

$$T(x) = b \int_x^L \int_{-\frac{h}{2}}^{\frac{h}{2}} \rho \tilde{\omega}^2 x dz dx. \tag{20}$$

In which, $\tilde{\omega}$ is the rotation speed of nanobeam. Motion equations can be derived by substituting Eqs. (15) to (17) into (11) based on MCST as follow:

$$\delta u : -m_0 \frac{\partial^2 u}{\partial t^2} - \bar{m}_1 \frac{\partial^2 \varphi}{\partial t^2} + c_1 m_3 \frac{\partial^3 w}{\partial x \partial t^2} + \frac{\partial M_{xx}^{(0)}}{\partial x} + f = 0, \tag{21a}$$

$$\delta \varphi : -\bar{m}_1 \frac{\partial^2 u}{\partial t^2} - \hat{m}_2 \frac{\partial^2 \varphi}{\partial t^2} + c_1 \bar{m}_4 \frac{\partial^3 w}{\partial x \partial t^2} + \frac{\partial \bar{M}_{xz}^{(1)}}{\partial x} - \bar{Q}_{xz}^{(0)} + \frac{\partial \bar{Y}_{yx}^{(0)}}{\partial x} + c_2 Y_{yz}^{(1)} = 0, \tag{21b}$$

$$\delta w : -m_0 \frac{\partial^2 w}{\partial t^2} - c_1 m_3 \frac{\partial^3 u}{\partial x \partial t^2} - c_1 \bar{m}_4 \frac{\partial^3 \varphi}{\partial x \partial t^2} + c_1^2 m_6 \frac{\partial^4 w}{\partial x^2 \partial t^2} + c_1 \frac{\partial^2 M_{xx}^{(3)}}{\partial x^2} + \frac{\partial \bar{Q}_{xz}^{(0)}}{\partial x} + \frac{\partial^2 \bar{Y}_{yx}^{(0)}}{\partial x^2} - c_2 \frac{\partial Y_{yz}^{(1)}}{\partial x} - \frac{\partial}{\partial x} \left(N_T \frac{\partial w}{\partial x} \right) + q - k_w w - k_d \frac{\partial w}{\partial t} + k_p \frac{\partial^2 w}{\partial x^2} + \frac{\partial}{\partial x} \left(T(x) \frac{\partial w}{\partial x} \right) = 0. \tag{21c}$$

5 Nonlocal (Eringen) theory

According to Eringen [33], the stress field at any random point x is a function of both strain field of that point (hyper-elastic case) and all other strain fields in the configuration. So, nonlocal stress tensor is denoted as:

$$\sigma = \int_V \kappa(|x' - x|, \eta) t(x') dx', \tag{22}$$

where $t(\cdot)$ indicates local stress tensor at point (\cdot) and $\kappa(|x' - x|, \eta)$ referees to nonlocal modulus. Thus, the general from of nonlocal characteristic equation is represented as [33]:

$$[1 - (e_0 a)^2 \nabla^2] t_{ij} = \lambda \varepsilon_{rr} \delta_{ij} + G \varepsilon_{ij}, \tag{23}$$

where t_{ij} and ε illustrate nonlocal stress and strain tensor, respectively, δ_{ij} is Kronecker delta, λ and G are Lamé's constants and $(e_0 a)^2$ denotes nonlocal parameter. Therefore, non-local constitutive relations can be expressed in the following forms [83]:

$$\sigma_{xx} - (e_0 a)^2 \frac{\partial^2 \sigma_{xx}}{\partial x^2} = E \varepsilon_{xx}, \tag{24a}$$

$$\sigma_{xz} - (e_0 a)^2 \frac{\partial^2 \sigma_{xz}}{\partial x^2} = 2G \varepsilon_{xz}, \tag{24b}$$

$$m_{yx} - (e_0a)^2 \frac{\partial^2 m_{yx}}{\partial x^2} = 2Gl_m^2 \chi_{yx}, \tag{24c}$$

$$m_{yz} - (e_0a)^2 \frac{\partial^2 m_{yz}}{\partial x^2} = 2Gl_m^2 \chi_{yz}. \tag{24d}$$

Using Eq. (10), nonlocal constitutive relations in Eqs. (24) can be developed as:

$$M_{xx}^{(0)} - (e_0a)^2 \frac{\partial^2 M_{xx}^{(0)}}{\partial x^2} = EI_0 \frac{\partial u}{\partial x}, \tag{25a}$$

$$\bar{M}_{xx}^{(1)} - (e_0a)^2 \frac{\partial^2 \bar{M}_{xx}^{(1)}}{\partial x^2} = E\bar{I}_2 \frac{\partial \varphi}{\partial x} - c_1 E\bar{I}_4 \left(\frac{\partial \varphi}{\partial x} + \frac{\partial^2 w}{\partial x^2} \right), \tag{25b}$$

$$M_{xx}^{(3)} - (e_0a)^2 \frac{\partial^2 M_{xx}^{(3)}}{\partial x^2} = EI_4 \frac{\partial \varphi}{\partial x} - c_1 EI_6 \left(\frac{\partial \varphi}{\partial x} + \frac{\partial^2 w}{\partial x^2} \right), \tag{25c}$$

$$\bar{Q}_{xz}^{(0)} - (e_0a)^2 \frac{\partial^2 \bar{Q}_{xz}^{(0)}}{\partial x^2} = G\bar{I}_0 \left(\varphi + \frac{\partial w}{\partial x} \right), \tag{25d}$$

$$\bar{Y}_{yx}^{(0)} - (e_0a)^2 \frac{\partial^2 \bar{Y}_{yx}^{(0)}}{\partial x^2} = \frac{1}{4} Gl_m^2 \left(I_0^* \left(\frac{\partial \varphi}{\partial x} - \frac{\partial^2 w}{\partial x^2} \right) - c_2 I_2^* \left(\frac{\partial \varphi}{\partial x} + \frac{\partial^2 w}{\partial x^2} \right) \right), \tag{25e}$$

$$\bar{Y}_{yx}^{(0)} - (e_0a)^2 \frac{\partial^2 \bar{Y}_{yx}^{(0)}}{\partial x^2} = \frac{1}{4} Gl_m^2 \left(\bar{I}_0 \left(\frac{\partial \varphi}{\partial x} - \frac{\partial^2 w}{\partial x^2} \right) - c_2 \bar{I}_2 \left(\frac{\partial \varphi}{\partial x} + \frac{\partial^2 w}{\partial x^2} \right) \right), \tag{25f}$$

$$Y_{yz}^{(1)} - (e_0a)^2 \frac{\partial^2 Y_{yz}^{(1)}}{\partial x^2} = -c_2 Gl_m^2 I_2 \left(\varphi + \frac{\partial w}{\partial x} \right), \tag{25g}$$

$$\bar{Q}_{xz}^{(0)} = -\bar{m}_1 \frac{\partial^2 u}{\partial t^2} - \hat{m}_2 \frac{\partial^2 \varphi}{\partial t^2} + c_1 \bar{m}_4 \frac{\partial^3 w}{\partial x \partial t^2} + \frac{\partial \bar{M}_{xx}^{(1)}}{\partial x} + \frac{\partial \bar{Y}_{yx}^{(0)}}{\partial x} + c_2 Y_{yz}^{(1)}, \tag{30}$$

$$\frac{\partial^2 \bar{Q}_{xz}^{(0)}}{\partial x^2} = -\bar{m}_1 \frac{\partial^4 u}{\partial x^2 \partial t^2} - \hat{m}_2 \frac{\partial^4 \varphi}{\partial x^2 \partial t^2} + c_1 \bar{m}_4 \frac{\partial^5 w}{\partial x^3 \partial t^2} + \frac{\partial^3 \bar{M}_{xx}^{(1)}}{\partial x^3} + \frac{\partial^3 \bar{Y}_{yx}^{(0)}}{\partial x^3} + c_2 \frac{\partial^2 Y_{yz}^{(1)}}{\partial x^2}. \tag{31}$$

in which:

$$I_i = \int_A z^i dA, \tag{26}$$

$$\bar{I}_i = I_i - c_1 I_{i+2}; \bar{\bar{I}}_i = I_i + c_2 I_{i+2}; \bar{\bar{I}}_i = \bar{I}_i - c_2 \bar{I}_{i+2}; I_i^* = I_i - c_2 I_{i+2}. \tag{27}$$

Calculating $\frac{\partial^2 M_{xx}^{(0)}}{\partial x^2}$ from Eq. (21a) yields:

$$\frac{\partial^2 M_{xx}^{(0)}}{\partial x^2} = m_0 \frac{\partial^3 u}{\partial x \partial t^2} + m_1 \frac{\partial^3 \varphi}{\partial x \partial t^2} - c_1 m_3 \frac{\partial^4 w}{\partial x^2 \partial t^2} - \frac{\partial f}{\partial x}. \tag{28}$$

By substituting Eq. (28) into Eq. (25a) and applying Eq. (21a), it is found that:

$$-m_0 \left[\frac{\partial^2 u}{\partial t^2} - (e_0a)^2 \frac{\partial^4 u}{\partial x^2 \partial t^2} \right] - m_1 \left[\frac{\partial^2 \varphi}{\partial t^2} - (e_0a)^2 \frac{\partial^4 \varphi}{\partial x^2 \partial t^2} \right] + c_1 m_3 \left[\frac{\partial^3 w}{\partial x \partial t^2} - (e_0a)^2 \frac{\partial^5 w}{\partial x^3 \partial t^2} \right] + \left[f - (e_0a)^2 \frac{\partial^2 f}{\partial x^2} \right] + EI_0 \frac{\partial^2 u}{\partial x^2} = 0. \tag{29}$$

Moreover, calculating $\bar{Q}_{xz}^{(0)}$ and $\frac{\partial^2 \bar{Q}_{xz}^{(0)}}{\partial x^2}$ from Eq. (21b) results in:

Substituting Eqs. (30) and (31) into Eq. (25d) and applying Eqs. (25b), (25e) and (25g) lead to:

$$\bar{m}_1 \left[\frac{\partial^2 u}{\partial t^2} - (e_0a)^2 \frac{\partial^4 u}{\partial x^2 \partial t^2} \right] + \hat{m}_2 \left[\frac{\partial^2 \varphi}{\partial t^2} - (e_0a)^2 \frac{\partial^4 \varphi}{\partial x^2 \partial t^2} \right] - c_1 \bar{m}_4 \left[\frac{\partial^3 w}{\partial x \partial t^2} - (e_0a)^2 \frac{\partial^5 w}{\partial x^3 \partial t^2} \right] + [G\bar{I}_0 + c_2^2 Gl_m^2 I_2] \varphi - \left[E\bar{I}_2 - \frac{1}{4} Gl_m^2 I_0' \right] \frac{\partial^2 \varphi}{\partial x^2} + [G\bar{I}_0 + c_2^2 Gl_m^2 I_2] \frac{\partial w}{\partial x} + \left[c_1 E\bar{I}_4 + \frac{1}{4} Gl_m^2 \bar{I}_0 \right] \frac{\partial^3 w}{\partial x^3} = 0. \tag{32}$$

Also, $\bar{Q}_{xz}^{(0)}$ can be obtained by calculating $\frac{\partial^2 \bar{Q}_{xz}^{(0)}}{\partial x^2}$ from Eq. (21c) and substituting it into Eq. (25d) as:

$$\bar{Q}_{xz}^{(0)} = (e_0a)^2 \left[\begin{aligned} & m_0 \frac{\partial^3 w}{\partial x \partial t^2} + c_1 m_3 \frac{\partial^4 u}{\partial x^2 \partial t^2} + c_1 \bar{m}_4 \frac{\partial^4 \varphi}{\partial x^2 \partial t^2} - c_1^2 m_6 \frac{\partial^5 w}{\partial x^3 \partial t^2} - c_1 \frac{\partial^3 M_{xx}^{(3)}}{\partial x^3} - \frac{\partial^2 \bar{Y}_{yx}^{(0)}}{\partial x^2} + \\ & c_2 \frac{\partial^2 Y_{yz}^{(1)}}{\partial x^2} - \frac{\partial^2}{\partial x^2} (N_T \frac{\partial w}{\partial x}) - \frac{\partial q}{\partial x} + K_w \frac{\partial w}{\partial x} + K_d \frac{\partial^2 w}{\partial x \partial t} - K_p \frac{\partial^3 w}{\partial x^3} - \frac{\partial^2}{\partial x^2} (T(x) \frac{\partial w}{\partial x}) \end{aligned} \right] + G\bar{I}_0(\varphi + \frac{\partial w}{\partial x}). \tag{33}$$

Substitution of the first derivative of $\bar{Q}_{xz}^{(0)}$ from Eq. (33) into Eq. (21c) and the application of Eqs. (25c), (25f) and (25g) results in:

where:

$$T_{\max} = \frac{1}{2} m_0 L^2 \bar{\omega}^2. \tag{37}$$

$$\begin{aligned} & -c_1 m_3 \left[\frac{\partial^3 u}{\partial x \partial t^2} - (e_0a)^2 \frac{\partial^5 u}{\partial x^3 \partial t^2} \right] - c_1 \bar{m}_4 \left[\frac{\partial^3 \varphi}{\partial x \partial t^2} - (e_0a)^2 \frac{\partial^5 \varphi}{\partial x^3 \partial t^2} \right] \\ & - \left[m_0 \frac{\partial^2 w}{\partial t^2} - (c_1^2 m_6 + (e_0a)^2 m_0) \frac{\partial^4 w}{\partial x^2 \partial t^2} + (e_0a)^2 c_1^2 m_6 \frac{\partial^6 w}{\partial x^4 \partial t^2} \right] - K_d \left[\frac{\partial w}{\partial t} - (e_0a)^2 \frac{\partial^3 w}{\partial x^2 \partial t} \right] \\ & + [G\bar{I}_0 + c_2^2 G_m^2 I_2] \frac{\partial \varphi}{\partial x} + \left[c_1 E \bar{I}_4 + \frac{1}{4} G_m^2 \bar{I}_0 \right] \frac{\partial^3 \varphi}{\partial x^3} - K_w w + \left[\frac{\partial T}{\partial x} - (e_0a)^2 \frac{\partial^3 T}{\partial x^3} \right] \frac{\partial w}{\partial x} \\ & + \left[G\bar{I}_0 + c_2^2 G_m^2 I_2 + K_p + (e_0a)^2 K_w - N_T + T - 3(e_0a)^2 \frac{\partial^2 T}{\partial x^2} \right] \frac{\partial^2 w}{\partial x^2} - \left[3(e_0a)^2 \frac{\partial T}{\partial x} \right] \frac{\partial^3 w}{\partial x^3} \\ & - \left[c_1^2 E I_6 + \frac{1}{4} G_m^2 I_0'' + (e_0a)^2 K_p + (e_0a)^2 T - (e_0a)^2 N_T \right] \frac{\partial^4 w}{\partial x^4} + q - (e_0a)^2 \frac{\partial^2 q}{\partial x^2} = 0. \end{aligned} \tag{34}$$

where:

$$\begin{aligned} \bar{I}'_i &= I_i^* - c_2 I_{i+2}^*; \bar{I}''_i = \bar{I}_i + c_2 \bar{I}_{i+2} \\ \hat{I}'_i &= \bar{I}_i - c_1 \bar{I}_{i+2}; \hat{I}''_i = I_i^* + c_2 I_{i+2}^* = \bar{I}_i - c_2 \bar{I}_{i+2}. \end{aligned} \tag{35}$$

Equations (29), (32) and (34) are motion equations in terms of generalized displacements. These equations are obtained by considering the effects of visco-elastic foundation, thermal forces and centrifugal stiffening due to the rotation of nanobeam.

To establish dimensionless motion equations, dimensionless parameters are achieved as the following:

Substituting Eq. (36) into Eqs. (29), (32) and (34) gives non-dimensional motion governing equations in terms of rotation and displacement as:

$$\begin{aligned} & \left[-\bar{M}_0 \frac{\partial^2 U}{\partial t^2} + \mu^2 \bar{M}_0 \frac{\partial^4 U}{\partial \zeta^2 \partial t^2} - \bar{M}_1 \frac{\partial^2 \Phi}{\partial t^2} \right. \\ & \left. + \mu^2 \bar{M}_1 \frac{\partial^4 \Phi}{\partial \zeta^2 \partial t^2} + \bar{M}_3 \frac{\partial^3 W}{\partial \zeta \partial t^2} - \mu^2 \bar{M}_3 \frac{\partial^5 W}{\partial \zeta^3 \partial t^2} \right] \\ & + \frac{\partial^2 U}{\partial \zeta^2} + \bar{f} - \mu^2 \frac{\partial^2 \bar{f}}{\partial \zeta^2} = 0, \end{aligned} \tag{38a}$$

$$\begin{aligned} \zeta &= \frac{x}{L}; \quad U = \frac{u}{L}; \quad W = \frac{w}{L}; \quad \Phi = \varphi; \quad \mu = \frac{e_0a}{L}; \quad l_0 = \frac{l_m}{h} \\ \bar{\tau} &= \frac{T}{T_{\max}}; \quad \bar{q} = \frac{qL}{EI_0}; \quad \bar{f} = \frac{fL}{EI_0}; \quad \vartheta = \frac{N_T}{EI_0}; \quad \Omega_w^2 = \frac{m_2 \omega^2}{EI_0} \\ \bar{M}_0 &= \frac{m_0 L^2}{m_2}; \bar{M}_1 = \frac{\bar{m}_1 L}{m_2}; \quad \bar{M}_2 = \frac{\hat{m}_2}{m_2}; \bar{M}_3 = \frac{c_1 m_3 L}{m_2}; \quad \bar{M}_4 = \frac{c_1 \bar{m}_4}{m_2}; \quad \bar{M}_6 = \frac{c_1^2 m_6}{m_2} \\ \alpha_0 &= \frac{G\bar{I}_0}{EI_0}; \quad \alpha_2 = \frac{E\hat{I}_2}{EI_0 L^2}; \quad \alpha_4 = \frac{c_1 E \bar{I}_4}{EI_0 L^2}; \quad \alpha_6 = \frac{c_1^2 E I_6}{EI_0 L^2} \\ \beta'_0 &= \frac{G_m^2 I_0'}{4EI_0 L^2}; \quad \beta''_0 = \frac{G_m^2 I_0''}{4EI_0 L^2}; \quad \beta_0 = \frac{G_m^2 I_0}{4EI_0 L^2}; \quad \beta_2 = \frac{c_2^2 G_m^2 I_2}{EI_0} \\ k_d &= \frac{K_d L^2}{\sqrt{EI_0 m_2}}; \quad k_w = \frac{K_w L^2}{EI_0}; \quad k_p = \frac{K_p}{EI_0}; \quad \mathfrak{S} = \frac{T_{\max}}{EI_0} \end{aligned} \tag{36}$$

$$\begin{aligned}
 & \left[\bar{M}_1 \frac{\partial^2 U}{\partial t^2} - \mu^2 \bar{M}_1 \frac{\partial^4 U}{\partial \zeta^2 \partial t^2} + \bar{M}_2 \frac{\partial^2 \Phi}{\partial t^2} \right. \\
 & \left. - \mu^2 \bar{M}_2 \frac{\partial^4 \Phi}{\partial \zeta^2 \partial t^2} - \bar{M}_4 \frac{\partial^3 W}{\partial \zeta \partial t^2} + \mu^2 \bar{M}_4 \frac{\partial^5 W}{\partial \zeta^3 \partial t^2} \right] \\
 & + [\alpha_0 + \beta_2] \Phi - [\alpha_2 + \beta'_0] \frac{\partial^2 \Phi}{\partial \zeta^2} \\
 & + [\alpha_0 + \beta_2] \frac{\partial W}{\partial \zeta} + [\alpha_4 + \tilde{\beta}_0] \frac{\partial^3 W}{\partial \zeta^3} = 0,
 \end{aligned} \tag{38b}$$

$$\begin{aligned}
 & \left[-\bar{M}_3 \frac{\partial^2 U}{\partial \zeta \partial t} + \mu^2 \bar{M}_3 \frac{\partial^5 U}{\partial \zeta^3 \partial t^2} - \bar{M}_4 \frac{\partial^3 \Phi}{\partial \zeta \partial t^2} + \mu^2 \bar{M}_4 \frac{\partial^5 \Phi}{\partial \zeta^3 \partial t^2} - \bar{M}_0 \frac{\partial^2 W}{\partial t^2} \right. \\
 & \quad \left. + (\bar{M}_6 + \mu^2 \bar{M}_0) \frac{\partial^4 W}{\partial \zeta^2 \partial t^2} - \mu^2 \bar{M}_6 \frac{\partial^6 W}{\partial \zeta^4 \partial t^2} \right] \\
 & + \left[-k_d \frac{\partial W}{\partial t} + \mu^2 k_d \frac{\partial^3 W}{\partial \zeta^2 \partial t} \right] + [\alpha_0 + \beta_2] \frac{\partial \Phi}{\partial \zeta} + [\alpha_4 + \tilde{\beta}_0] \frac{\partial^3 \Phi}{\partial \zeta^3} - k_w W \\
 & + \mathfrak{S} \left[\frac{\partial \bar{\tau}}{\partial \zeta} - \mu^2 \frac{\partial^3 \bar{\tau}}{\partial \zeta^3} \right] \frac{\partial W}{\partial \zeta} + \left[\mathfrak{S} \bar{\tau} - 3\mu^2 \mathfrak{S} \frac{\partial^2 \bar{\tau}}{\partial \zeta^2} + \alpha_0 + \beta_2 + k_p + \mu^2 k_w - \vartheta \right] \frac{\partial^2 W}{\partial \zeta^2} \\
 & - \left[3\mu^2 \mathfrak{S} \frac{\partial \bar{\tau}}{\partial \zeta} \right] \frac{\partial^3 W}{\partial \zeta^3} - [-\mu^2 \mathfrak{S} \bar{\tau} + \alpha_6 + \beta''_0 + \mu^2 k_p - \mu^2 \vartheta] \frac{\partial^4 W}{\partial \zeta^4} + \bar{q} - \mu^2 \frac{\partial^2 \bar{q}}{\partial \zeta^2} = 0.
 \end{aligned} \tag{38c}$$

6 Solution procedure

In this section, the analytical solutions of wave propagation governing equations of rotating viscoelastic nanobeams resting on elastic foundations under thermal effects are described. Adopting harmonic method, wave propagation displacement fields are defined as [84]:

$$\begin{Bmatrix} U(\zeta, t) \\ W(\zeta, t) \\ \Phi(\zeta, t) \end{Bmatrix} = \begin{Bmatrix} U_0 \exp[i(K\zeta - \Omega_w t)] \\ W_0 \exp[i(K\zeta - \Omega_w t)] \\ \Phi_0 \exp[i(K\zeta - \Omega_w t)] \end{Bmatrix}, \tag{39}$$

$$\mathbf{M} = \begin{bmatrix} m_{U_0 U_0} & m_{U_0 \Phi_0} & m_{U_0 W_0} \\ m_{\Phi_0 U_0} & m_{\Phi_0 \Phi_0} & m_{\Phi_0 W_0} \\ m_{W_0 U_0} & m_{W_0 \Phi_0} & m_{W_0 W_0} \end{bmatrix}; \quad \mathbf{K} = \begin{bmatrix} k_{U_0 U_0} & k_{U_0 \Phi_0} & k_{U_0 W_0} \\ k_{\Phi_0 U_0} & k_{\Phi_0 \Phi_0} & k_{\Phi_0 W_0} \\ k_{W_0 U_0} & k_{W_0 \Phi_0} & k_{W_0 W_0} \end{bmatrix}; \quad \mathbf{C} = \begin{bmatrix} c_{U_0 U_0} & c_{U_0 \Phi_0} & c_{U_0 W_0} \\ c_{\Phi_0 U_0} & c_{\Phi_0 \Phi_0} & c_{\Phi_0 W_0} \\ c_{W_0 U_0} & c_{W_0 \Phi_0} & c_{W_0 W_0} \end{bmatrix}. \tag{41}$$

Table 1 Material properties

<i>E</i> (GPa)	<i>G</i> (GPa)	<i>ν</i>	<i>ρ</i> (kg/m ³)	<i>α</i> (°C ⁻¹)	<i>h</i> (nm)
210	80	0.3	7800	12.33e-6	1

where Ω_w and K are non-dimensional circular frequency and non-dimensional wave number, respectively, $X = (U_0, W_0, \Phi_0)$ is wave amplitude and $i = \sqrt{-1}$. Since in this work wave propa-

gation is considered in unbounded elastic domains, boundary conditions cannot be taken into account [85–88].

By substituting Eq. (39) and its derivatives into Eqs. (38), the characteristic equation is extracted as:

$$(\mathbf{K} + \Omega_w \mathbf{C} + \Omega_w^2 \mathbf{M}) \mathbf{X} = 0, \tag{40}$$

where \mathbf{M} , \mathbf{K} and \mathbf{C} are mass, stiffness and damping matrices, respectively, and include complex terms:

In which:

$$\begin{aligned}
 m_{U_0 U_0} &= \bar{M}_0(1 + \mu^2 K^2); \quad m_{U_0 \Phi_0} = \bar{M}_1(1 + \mu^2 K^2); \quad m_{U_0 W_0} = -i\bar{M}_3 K(1 + \mu^2 K^2) \\
 m_{\Phi_0 U_0} &= -\bar{M}_1(1 + \mu^2 K^2); \quad m_{\Phi_0 \Phi_0} = -\bar{M}_2(1 + \mu^2 K^2); \quad m_{\Phi_0 W_0} = i\bar{M}_4 K(1 + \mu^2 K^2) \\
 m_{W_0 U_0} &= i\bar{M}_3 K(1 + \mu^2 K^2); \quad m_{W_0 \Phi_0} = i\bar{M}_4 K(1 + \mu^2 K^2); \quad m_{W_0 W_0} = (\bar{M}_0 + K^2 \bar{M}_6)(1 + \mu^2 K^2) \\
 k_{U_0 U_0} &= -K^2; \quad k_{U_0 \Phi_0} = k_{\Phi_0 U_0} = k_{U_0 W_0} = k_{W_0 U_0} = 0; \\
 k_{\Phi_0 \Phi_0} &= (\alpha_0 + \beta_2) + (\alpha_0 + \beta'_0) K^2; \quad k_{\Phi_0 W_0} = k_{W_0 \Phi_0} = iK \left[(\alpha_0 + \beta_2) - (\alpha_4 + \tilde{\beta}_0) K^2 \right] \\
 k_{W_0 W_0} &= -k_w + i\mathfrak{S} \left(\frac{\partial \bar{\tau}}{\partial \zeta} - \mu^2 \frac{\partial^3 \bar{\tau}}{\partial \zeta^3} \right) K - \left(\mathfrak{S} \bar{\tau} - 3\mu^2 \mathfrak{S} \frac{\partial^2 \bar{\tau}}{\partial \zeta^2} + \alpha_0 + \beta_2 + k_p + \mu^2 k_w - \vartheta \right) K^2 \\
 & \quad - i(3\mu^2 \mathfrak{S} \frac{\partial \bar{\tau}}{\partial \zeta}) K^3 + (\alpha_6 + \beta''_0 + \mu^2 k_p - \mu^2 \vartheta - \mu^2 \mathfrak{S} \bar{\tau}) K^4 \\
 c_{W_0 W_0} &= ik_d(1 + \mu^2 K^2); \quad c_{U_0 U_0} = c_{U_0 \Phi_0} = c_{U_0 W_0} = c_{\Phi_0 U_0} = c_{\Phi_0 \Phi_0} = c_{\Phi_0 W_0} = c_{W_0 U_0} = c_{W_0 \Phi_0} = 0.
 \end{aligned} \tag{42}$$

Also, it is obvious that: $m_{U_0\Phi_0} = m_{U_0W_0} = m_{\Phi_0U_0} = m_{W_0U_0} = 0$.

The standard form for eigenvalue problem solution in Eq. (40) is:

$$\begin{bmatrix} -M^{-1}C & -M^{-1}K \\ I & 0 \end{bmatrix} \begin{Bmatrix} \dot{X} \\ X \end{Bmatrix} = \Omega_w \begin{Bmatrix} \dot{X} \\ X \end{Bmatrix}. \tag{43}$$

Equation (43) is an eigenvalue problem in which, by setting the determinant of the above matrix to zero, TA, LA and TO wave frequencies can be easily estimated. In addition, phase velocities of waves can be simply calculated by $c = \Omega_w/K$.

7 Numerical results and discussions

In this section, numerical results are obtained and evaluated for the wave propagation of rotating viscoelastic nanobeams considering the variations of the six parameters of $\frac{e_0a}{l_m}, k_w, k_p, \Delta T, \Omega_b$ and $\frac{L}{h}$. Also, the effects of the ratio of non-local to length scale $\frac{e_0a}{l_m}$, non-dimensional Winkler and Pasternak coefficients k_w and k_p , temperature gradient ΔT , non-dimensional beam rotating velocity Ω_b and slenderness ratio $\frac{L}{h}$ are described. Therefore, we kept five out of six parameters constant in each step and changed the value of the remaining parameter to evaluate parameter effects and interactions. The thermo-mechanical characteristics of rotating viscoelastic nanobeams are given in Table 1.

The results obtained for three TO, TA and LA wave propagation types in nano beams are illustrated and discussed in detail.

8 Model validation

For the validation of the developed model and accuracy verification of the findings, numerical results are obtained based on NL-MCST model with materials of Ref. [74] and compared with those reported in the mentioned reference. To this end, we reduced the presented NL-MCST into NL by considering $l_m = 0$. Also, we used mechanical properties given in Ref. [74] considering $n_x = n_z = \gamma = 0$ to establish the results for comparison and model validation. The results are compared for two different slenderness ratios ($\frac{L}{h} = 10$ and 15) and three different values of nonlocal parameter $e_0a = 1, 2$ and 3(nm). Comparison results are summarized in Table 2 for all TA, LA and TO wave propagation types. The comparison results given in Table 2 show good agreement between the results obtained by the developed method and those reported in Ref. [74] verifying the accuracy of our model.

8.1 Effects of e_0a and l_m

Figure 2 illustrates the trends of TO, TA and LA wave propagation frequencies based on non-dimensional wave number. As can be seen, by the increase of non-dimensional wave

Table 2 Model validation by comparison of frequencies for three types of wave propagation (THz) ($\Delta T = k_w = k_p = 0$ and $\Omega_b = 2$ Grad/s)

		e_0a (nm)	TA-Wave		LA-Wave		TO-Wave	
			Ref. [74]	Present Model	Ref. [74]	Present Model	Ref. [74]	Present model
$l_m = 0$ and $\frac{L}{h} = 10$	$K = 1(\text{nm})^{-1}$	1	0.8613	0.8609	9.0997	9.0995	3.3147	3.3147
		2	0.5447	0.5445	5.7552	5.7550	2.0964	2.0964
		3	0.3852	0.3851	4.0695	4.0695	1.4824	1.4824
	$K = 3(\text{nm})^{-1}$	1	2.2998	2.2997	6.1578	6.1577	4.4472	4.4470
		2	1.1956	1.1954	3.2013	3.2011	2.3120	2.3121
		3	0.8031	0.8030	2.1504	2.1504	1.5530	1.5530
	$K = 5(\text{nm})^{-1}$	1	2.8201	2.8202	5.4038	5.4040	4.5967	4.5967
		2	1.4308	1.4306	2.7417	2.7419	2.3323	2.3325
		3	0.9565	0.9566	1.8329	1.8325	1.5591	1.5592
$l_m = 0$ and $\frac{L}{h} = 15$	$K = 1(\text{nm})^{-1}$	1	0.6064	0.6065	12.9216	12.9209	3.3148	3.3147
		2	0.3835	0.3833	8.1723	8.1722	2.0964	2.0964
		3	0.2712	0.2706	5.7787	5.7788	1.4824	1.4824
	$K = 3(\text{nm})^{-1}$	1	1.8817	1.8814	7.5085	7.5081	4.4472	4.4471
		2	0.9782	0.9781	3.9035	3.9033	2.3120	3.3120
		3	0.6571	0.6572	2.6220	2.6220	1.5530	1.5531
	$K = 5(\text{nm})^{-1}$	1	2.4792	2.4792	6.1086	6.1087	4.5968	4.5967
		2	1.2579	1.2581	3.0993	3.0992	2.3323	2.3325
		3	0.8409	0.8408	2.0719	2.0720	1.5591	1.5592

Fig. 2 Wave propagation frequencies based on NL and NL-MCSTs. **a** Longitudinal (LA) waves. **b** Transverse (TA) wave. **c** Torsional (TO) wave. ($\Delta T = k_w = k_p = \Omega_b = 0$)

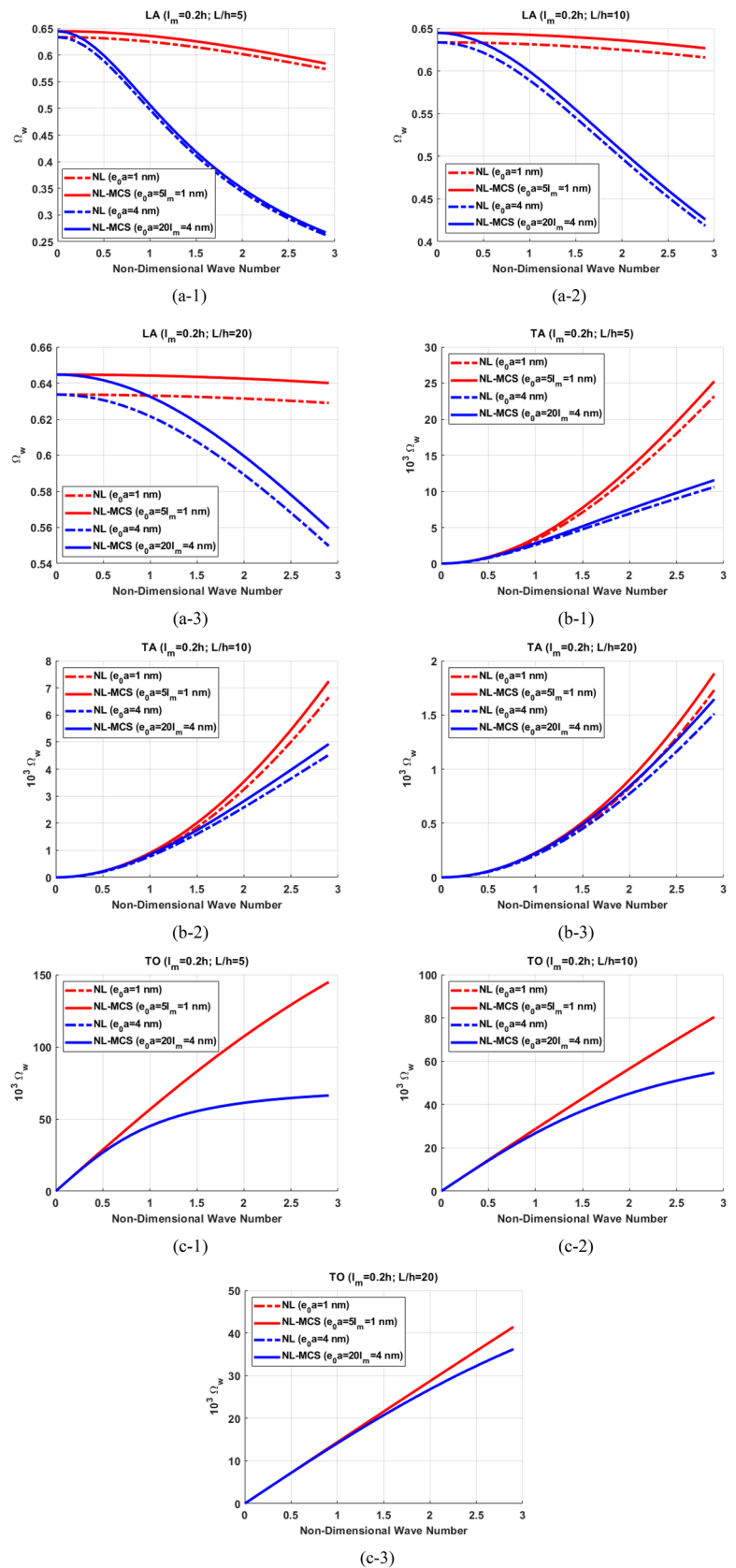
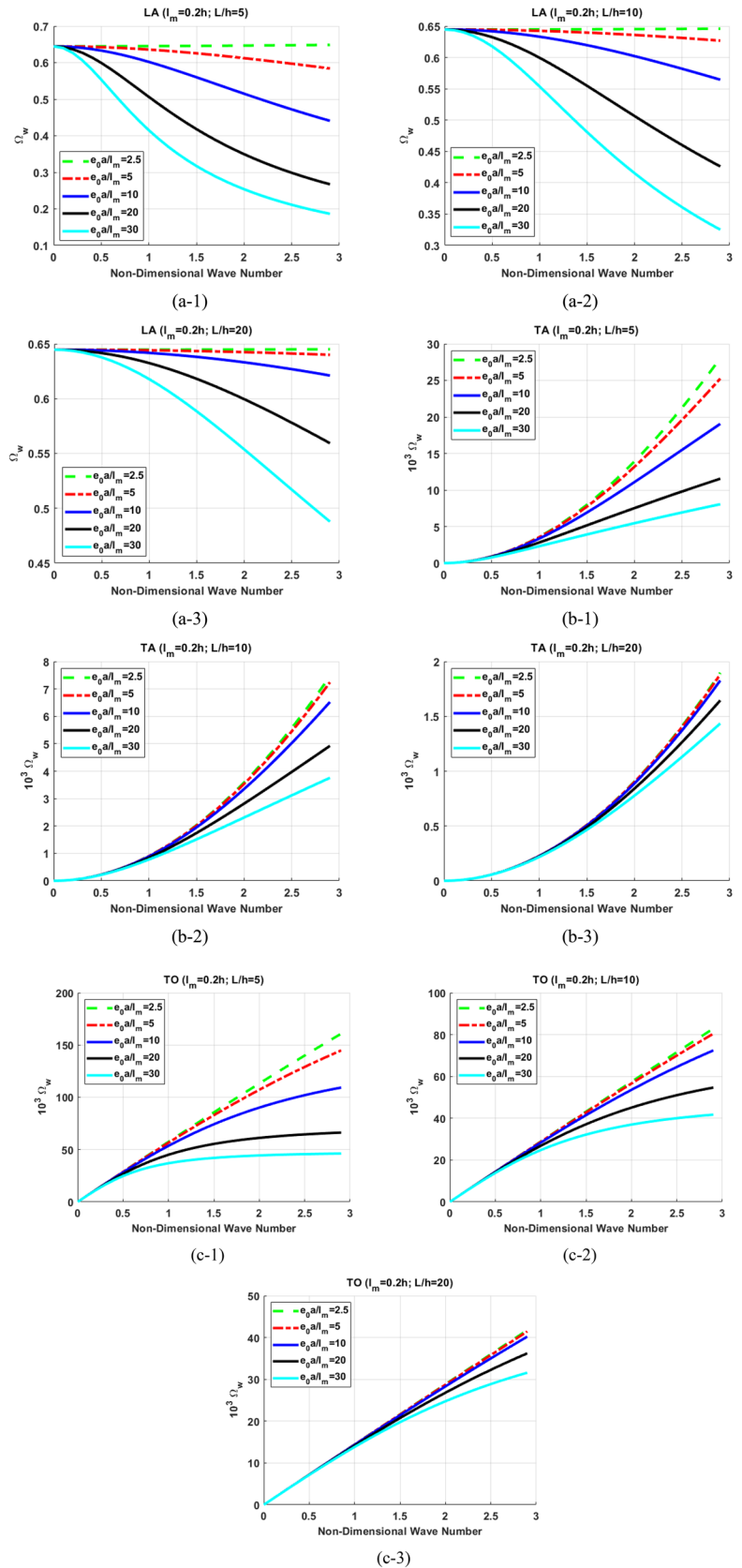


Fig. 3 Wave propagation frequencies for different nonlocal parameter to length scale ratios. **a** Longitudinal (LA) wave. **b** Transverse (TA) wave. **c** Torsional (TO) wave. ($\Delta T = k_w = k_p = \Omega_b = 0$)



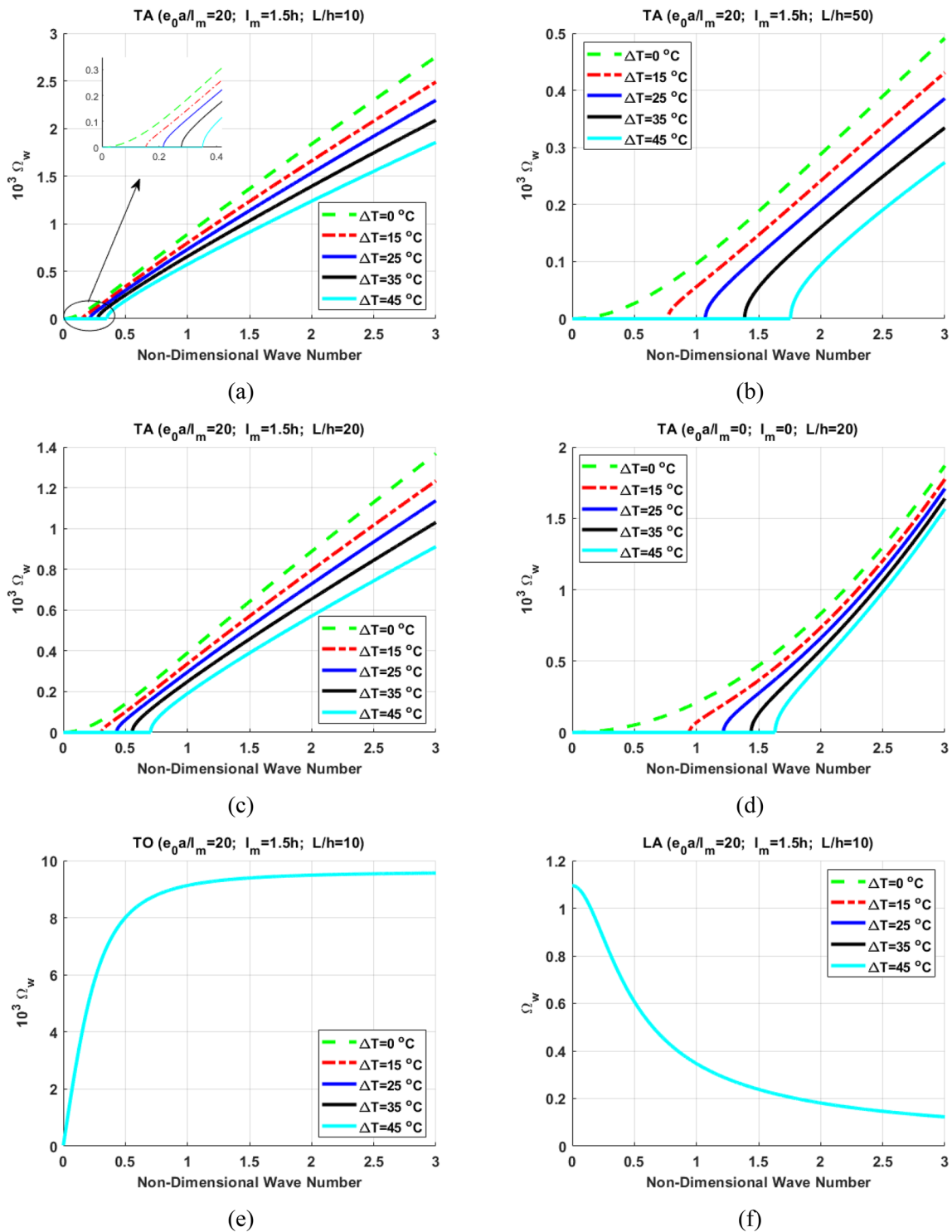


Fig. 4 Wave propagation frequencies for different temperatures. **a–d** Transverse (TA) wave. **e** Torsional (TO) wave. **f** Longitudinal (LA) wave. ($k_w = k_p = \Omega_b = 0$)

number, LA wave propagation frequency is decreased but for TA and TO wave propagations, the values of non-dimensional frequencies are increased.

Also, Fig. 2 presents the comparison of wave propagation fundamental frequencies extracted by Eringen’s nonlocal (NL) and nonlocal modified couple stress (NL-MCST) theories. As is clear, for LA and TA wave propagations,

the results obtained by NL-MCST were higher than those obtained by NL for all non-dimensional wave number. However, there was no difference between NL and NL-MCST results for TO wave propagation. The results obtained for LA and TA wave propagations show that for the same value of e_0a in NL and NL-MCST, the effect of length parameter l_m on NL-MCST increases wave propagation frequency but has no effect on wave propagation. Also, it can be concluded that, for LA wave propagation, increase of non-dimensional wave number decreases the difference between NL and NL-MCST wave frequencies whereas for TA wave propagation, this is opposite.

The effects of different nonlocal parameter to length scale ratios e_0a/l_m on non-dimensional fundamental wave propagation frequency for all wave propagation types are

indicated in Fig. 3. The results shown here are obtained by three different slenderness ratios of $L/h = 5, 10$ and 20 . As it is obvious from the figure and due to the decrease of stiffness, TO, TA and LA wave frequencies decrease with the increase of e_0a/l_m . Also, by increasing slenderness ratio, frequency difference for different e_0a/l_m ratios decreases.

8.2 Effects of temperature

Figure 4 displays the effect of temperature variation on non-dimensional frequencies of LA, TA and TO wave propagations.

In this section, $T_0 = 20^\circ\text{C}$ is considered as the reference temperature and temperature variation is considered at five different levels from $\Delta T = 0^\circ\text{C}$ to $\Delta T = +45^\circ\text{C}$. According

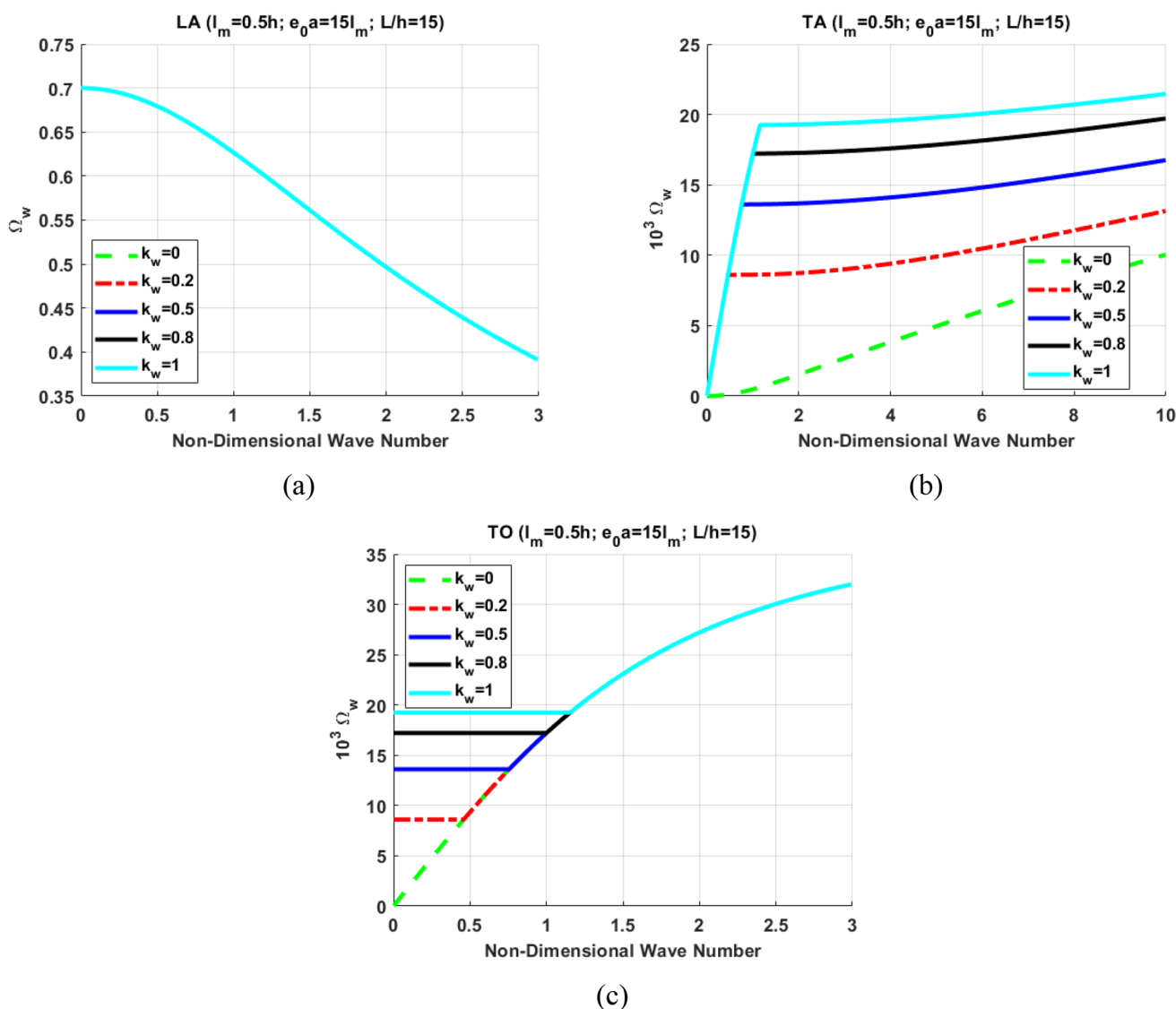


Fig. 5 Wave propagation frequencies for different non-dimensional Winkler coefficients. **a** Longitudinal (LA) waves. **b** Transverse (TA) wave. **c** Torsional (TO) wave. ($\Delta T = k_p = \Omega_b = 0$)

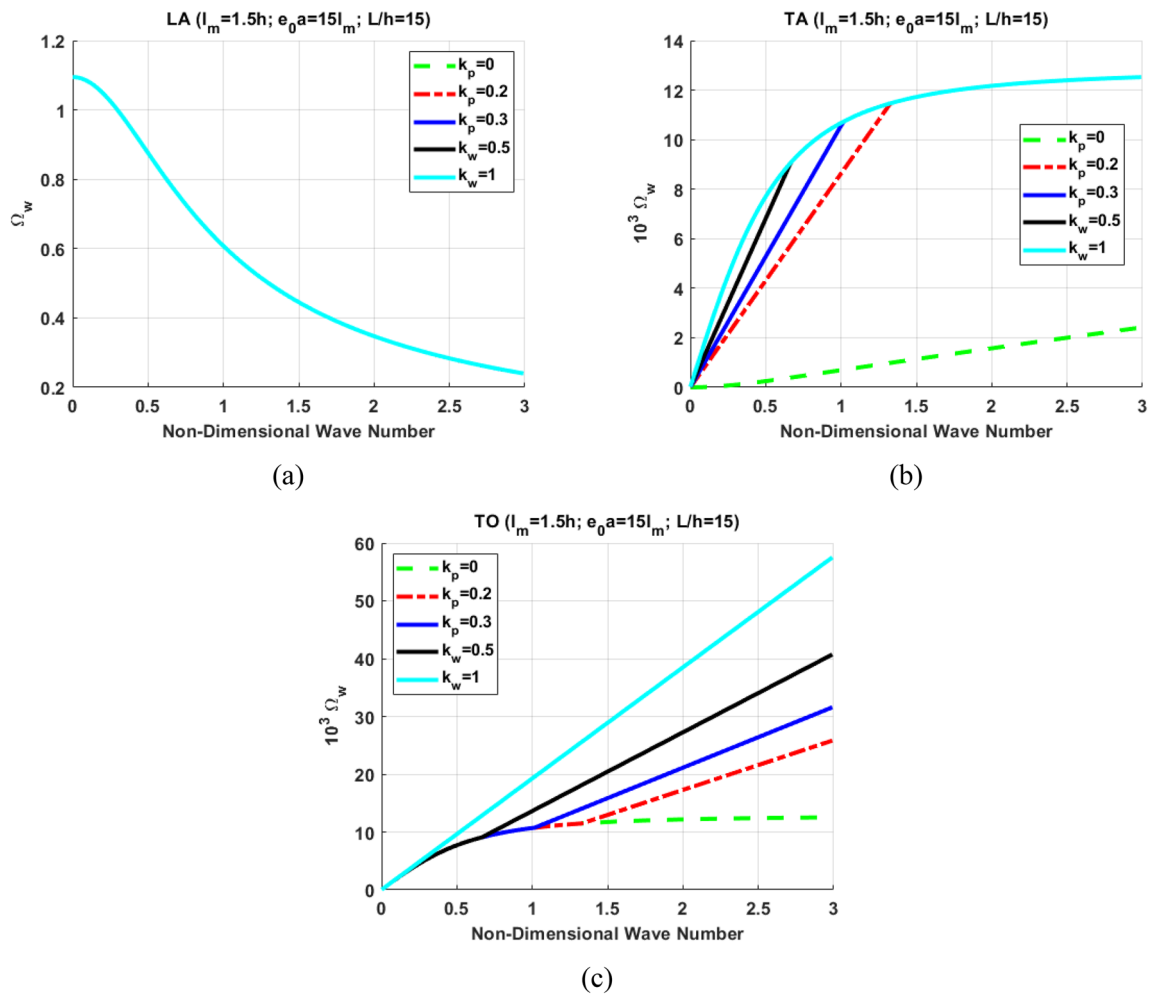


Fig. 6 Wave propagation frequencies for different non-dimensional Pasternak coefficients. **a** Longitudinal (LA) wave. **b** Transverse (TA) wave. **c** Torsional (TO) wave. ($\Delta T = k_w = \Omega_b = 0$)

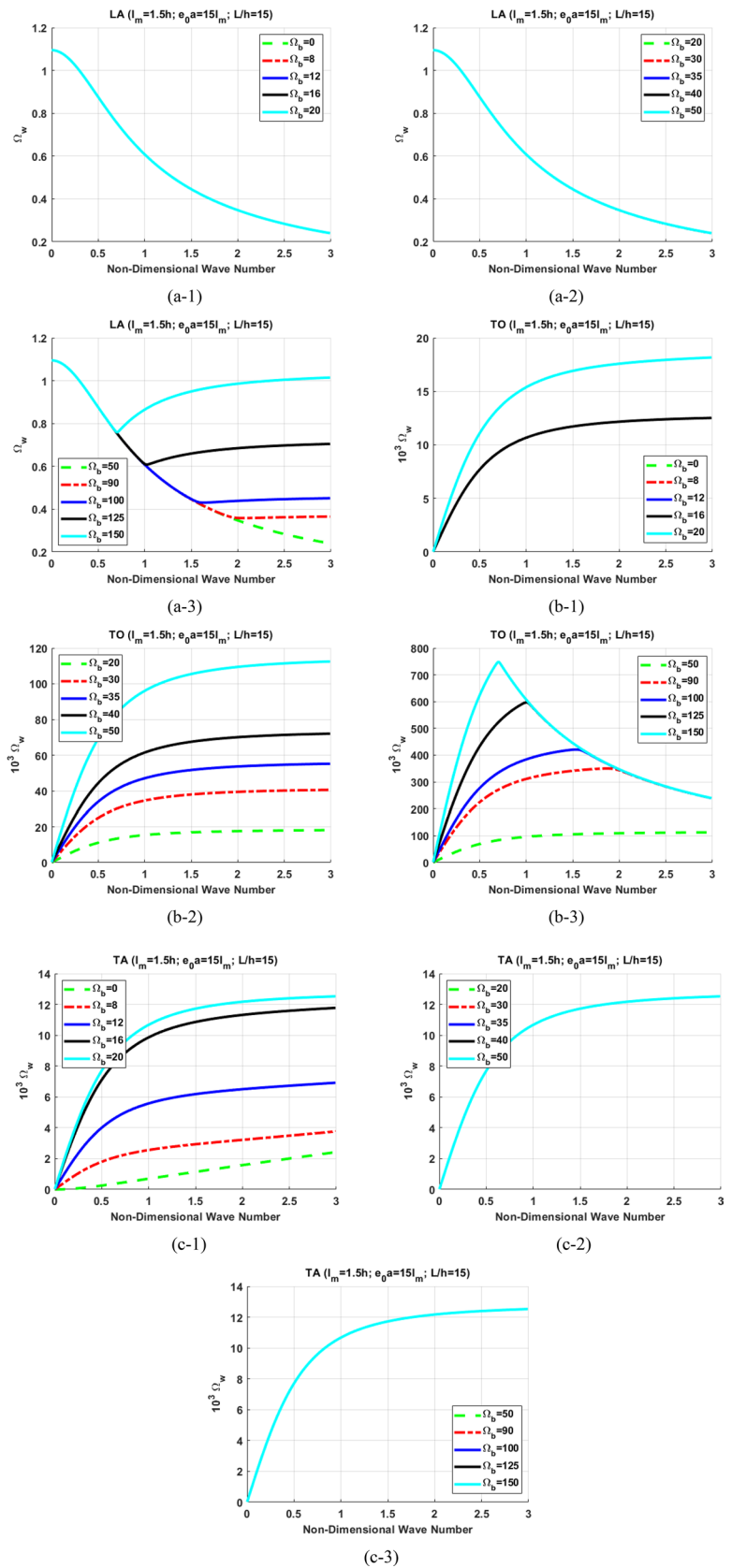
to Fig. 4, temperature gradient has no significant effects on TO and LA wave propagations. However, it strongly affects TA wave propagation. Figure 4a–c show TA wave frequencies for constant values of $e_0 a/l_m = 20$ and $l_m = 1.5h$ and different slenderness ratio values of $L/h = 10, 20$ and 50 . Also, Fig. 4d shows the results obtained for local case with $e_0 a = l_m = 0$ and $L/h = 20$. Based on the results obtained for TA wave propagation, with the increase of temperature, the initiation of TA wave propagation is delayed. Moreover, an increase in temperature reduces the value of TA wave frequencies. Also, with increasing slenderness ratio, wave propagation delay due to increasing temperature gradient increases.

8.3 Effects of Winkler-Pasternak coefficients

In this section, Winkler coefficient effect on non-dimensional wave frequency is considered. The effect of dimensionless Winkler coefficient k_w on all types of wave propagation is

presented in Fig. 5. The results are obtained for the constant values of $e_0 a/l_m = 15$, $l_m = 0.5h$ and $L/h = 15$ but different values of $0 \leq k_w \leq 1$ in five steps. As it is clear, LA wave propagation is not affected by different values of k_w and indicates the same behavior for all values of k_w . However, the variation of k_w has considerable effects on TO and TA wave propagations. In TA wave and for $k_w > 0$, with the increase of non-dimensional wave number up to a certain value, frequency is not affected by k_w but for higher non-dimensional wavenumbers, frequency trend is changed. It is obvious that the increase of k_w increases the value of TA wave frequency. For TO wave type, by increasing k_w , the wave propagation initiates with high frequencies. Also, TO frequency remains constant up to certain value of non-dimensional wave number but for higher non-dimensional wavenumbers, frequency trend tracks similar paths to that of $k_w = 0$. In other words, the variation of k_w above a certain value of non-dimensional wave number has no considerable influence on wave frequency.

Fig. 7 Wave propagation frequencies for different beam rotating velocity. **a** Longitudinal (LA) wave. **b** Torsional (TO) wave. **c** Transverse (TA) wave. ($\Delta T = k_w = k_p = 0$)



Pasternak coefficient effect on the non-dimensional frequency of all wave propagation types is illustrated in Fig. 6. Similar to the effect of k_w on LA wave, different values of k_p has no effect on frequency. However, the effects of k_p on TO and TA wave propagations is slightly different from that of k_w which is clear in Fig. 6. It can be concluded that, with the increase of k_p from 0 to 1, TA frequency increases. For $k_p > 0$, frequency difference is affected by the value of non-dimensional wave number. In other words, for $k_p > 0$ and higher non-dimensional wavenumbers (here $K > 1.3$), all frequencies converge to the same trend as that of $k_p = 1$ (Fig. 6b). For TO wave frequency and with increasing k_p , first, the frequency trend up to certain value of non-dimensional wave number follows the same trend of $k_p = 0$. Then, for higher non-dimensional wave numbers, TO frequency increases with increasing k_p (Fig. 2c).

8.4 Effects of beam rotating velocity

In this section, the effects of dimensionless rotating velocities of viscoelastic nanobeams Ω_b on all types of wave propagations are considered. Dimensionless beam rotating velocity is defined as:

$$\Omega_b = \tilde{\omega} L^2 \sqrt{\frac{\rho A}{EI}}, \tag{44}$$

where $A, \tilde{\omega}, L, I$ are cross-section area, beam rotating velocity, length, and second moment of cross-section area, respectively, E is Young’s modulus and ρ is the density of beam.

The effects of Ω_b on TO, TA and LA wave propagations are presented in Fig. 7. The results are obtained for constant values of $e_0 a / l_m = 15, l_m = 1.5h$ and $L/h = 15$. Also, to perform a comprehensive investigation on the effect of dimensionless rotating velocity on wave propagation,

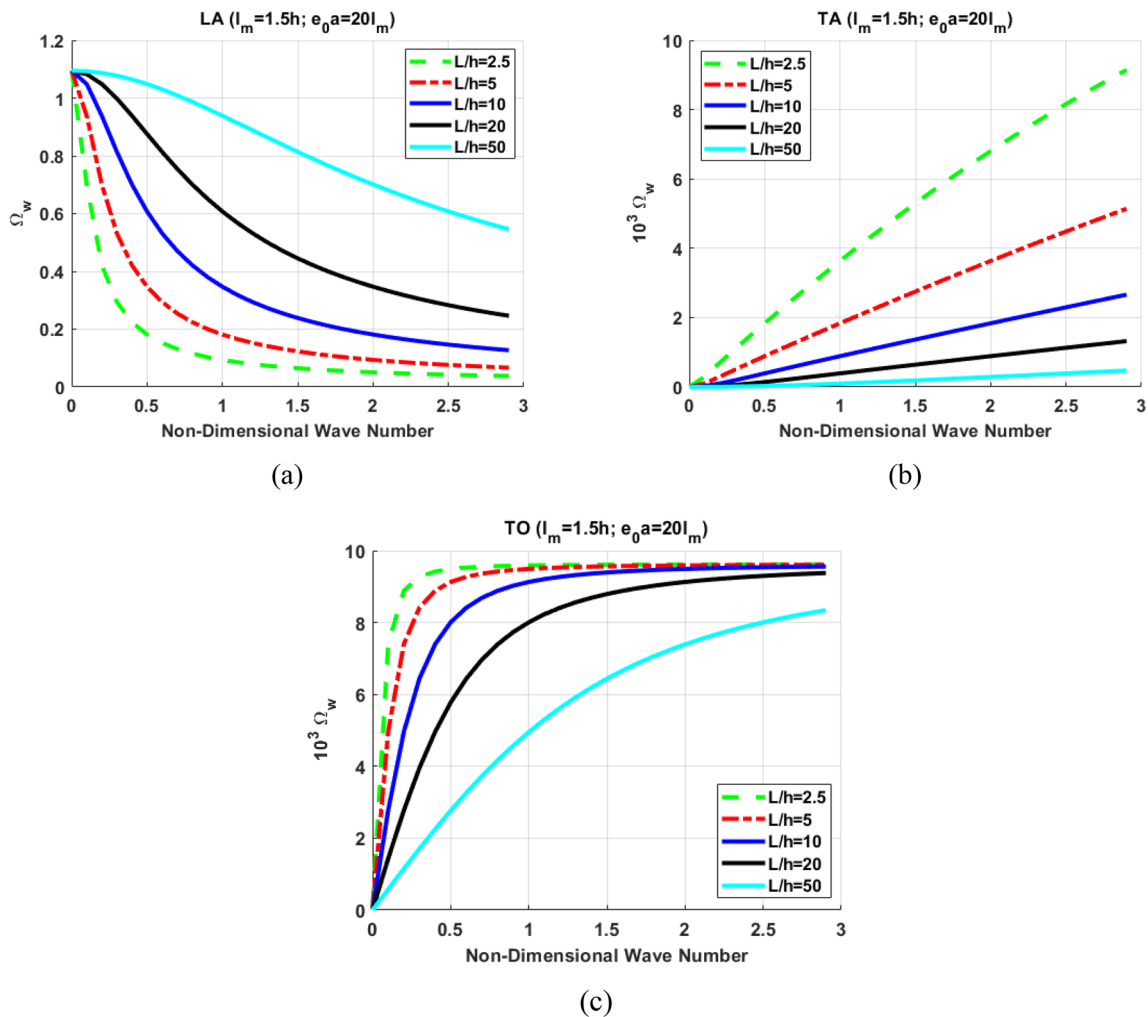


Fig. 8 Wave propagation frequencies based on different slenderness ratio. **a** Longitudinal (LA) Waves. **b** Transverse (TA) Wave. **c** Torsional (TO) Wave. ($\Delta T = k_w = k_p = \Omega_b = 0$)

rotating velocity Ω_b is applied in three different categories $0 \leq \Omega_b \leq 20$, $20 \leq \Omega_b \leq 50$ and $50 \leq \Omega_b \leq 150$. For LA wave propagations illustrated in graphs (a-1) to (a-3) of Fig. 7, the increase of Ω_b up to $\Omega_b = 50$ has no effect on wave frequency and it shows descending trend for all

$\Omega_b \leq 50$. However, for $50 < \Omega_b \leq 150$ and after a certain value of non-dimensional wave number, the descending trend is stopped and presents constant or ascending behaviors, as indicated in the Fig. 7a-3.

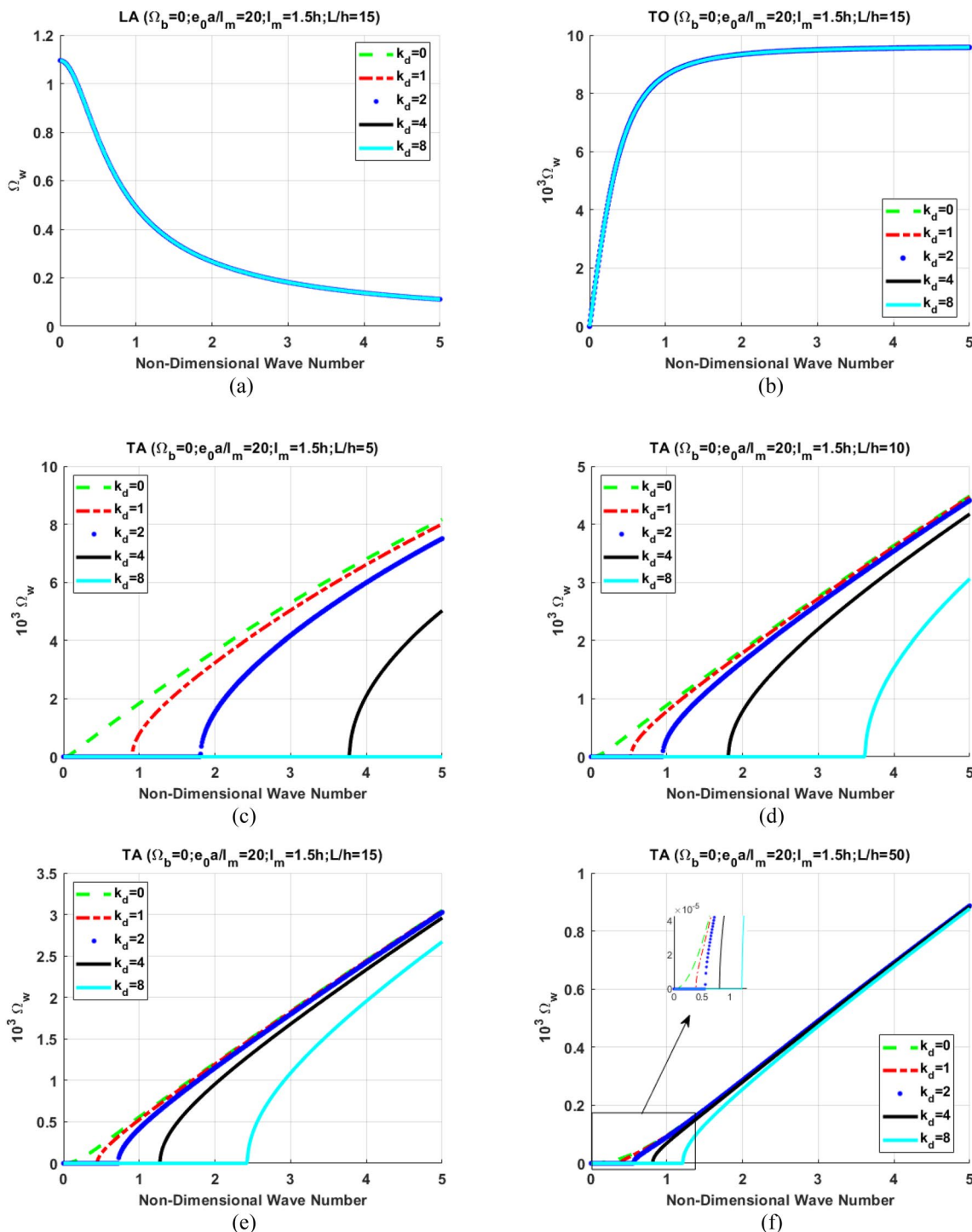


Fig. 9 Wave propagation frequencies based on different visco-damping coefficient. **a** Longitudinal (LA) Waves. **b** Torsional (TO) Wave. **c–f** Transverse (TA) Wave with different slenderness ratio. ($\Delta T = k_w = k_p = \Omega_b = 0$)

Also, in TO wave propagations displayed in graphs (b-1) to (b-3) of Fig. 7, $\Omega_b \leq 16$ has no effect on wave frequency. On the other hand, the increase of Ω_b has dual effects on wave frequency. For $20 \leq \Omega_b \leq 50$, wave frequency has a strictly ascending trend. However, for $\Omega_b > 50$, the trend is ascending up to a certain value of non-dimensional wave number and then it descends and then tracks identical trend.

Graphs (c-1) to (c-3) of Fig. 7 indicate the effect of Ω_b on TA waves. It can be concluded that, only for $\Omega_b \leq 20$, the frequency of TA wave propagation increases by the increase of Ω_b . However, high values of $\Omega_b > 20$ has no significant influence on TA wave frequency.

8.5 Effects of slenderness ratio

Figure 8 shows the effects of slenderness ratio on all types of wave propagation. The results are illustrated for constant values of $e_0 a/l_m = 20$, $l_m = 1.5h$. To obtain the results, the value of slenderness ratio was varied from 2.5 to 50 in five steps. According to the obtained results for TA wave propagation, slenderness ratio has considerable effects at all non-dimensional wavenumbers. However, in LA and TO waves and for high non-dimensional wavenumbers, frequencies reach a constant value above which slenderness ratio has no significant effect. As shown, with the increase of slenderness ratio, the frequencies of TA and TO wave propagation types decrease but that of TA type increases. It is obvious that, by the increase of slenderness ratio, frequency gradient becomes smoother for all types of wave propagation. In other words, with the increase of slenderness ratio, the frequencies of LA and TA types of wave propagation reach to a constant value in higher non-dimensional wave numbers.

8.6 Effects of slenderness ratio

The effect of non-dimensional visco-damping coefficient k_d on all types of wave propagation is illustrated in Fig. 9. The results are extracted based on different non-dimensional visco-damping coefficient values of $k_d = 0, 1, 2, 4$ and 8 for, LA, TO and TA types of wave propagation. It can be concluded easily that, the variation of k_d only affects the TA type of wave and has no effect on To and LA types of wave propagation. Also, it is clear from Fig. 9c–f that, wave propagation for TA type is postponed by the increment of the value of k_d . For example, in Fig. 9c, until non-dimensional wave number K reaches 5, the TA type of wave for $k_d = 8$ has not propagated. However, the wave propagates for $k_d = 0, 1, 2$ and 4 before $K = 5$.

On the other hand, at the same value of non-dimensional wave number, wave frequency for TA type decreases with increasing the value of k_d . Finally, by increasing the value of L/h , the TA type of wave will propagate in small value of non-dimensional wave number. Also, with the increase of

slenderness ratio, the increment of k_d value loses its effect on the frequency of TA type of wave for higher non-dimensional wave numbers.

9 Conclusion

The aim of this research was to develop a comprehensive mathematical-mechanical model for the investigation of wave propagations in rotating viscoelastic nanobeams resting on Winkler-Pasternak foundations considering thermal effects. In this work, to capture both hardening and softening behaviors of materials in wave propagation, nonlocal Eringen's and modified couple stress theories are incorporated to obtain governing equations of motion. In addition, higher order shear deformation beam model is applied to obtain motion equations and an analytic method is utilized to solve them. The results are illustrated for LA, TA and TO wave propagations and are discussed in detail. Moreover, the effects of nonlocal parameter to length scale ratios, thermal gradient, Winkler-Pasternak coefficients, rotating velocity of viscoelastic nanobeams and slenderness ratios are captured and are comprehensively discussed. The following major conclusions were drawn:

- By increasing non-dimensional wave number, LA wave propagation frequency decreases but, for TA and TO wave propagation types, the value of non-dimensional frequency increases.
- For LA and TA wave propagation types, the results obtained from NL-MCST are higher than those of NL for all non-dimensional wavenumbers. On the other hand, there is no difference between NL and NL-MSCT results for TO wave propagation.
- LA, TA and TO types of wave frequencies decrease with the increase of $e_0 a/l_m$.
- Temperature gradient has no significant effects on LA and TO wave propagations. However, it strongly affects TA wave propagation.
- With the increase of temperature, TA wave propagation is delayed. Also, increase of temperature reduces TA wave frequency.
- LA wave propagation is not affected by different values of k_w and k_p . However, the variation of k_w and k_p have considerable effects on TO and TA wave propagations.
- The frequencies of TA wave propagations are affected only at $\Omega_b \leq 20$.
- The increase of Ω_b has dual effects on TA and TO wave frequencies.
- With the increase of slenderness ratio, the frequencies of TA and TO wave propagations decrease but that of TA type increases.

- The variation of non-dimensional visco-damping coefficient affects only the TA type of wave propagation.
- For the same value of the non-dimensional wave number, the wave frequency of TA type decreases with increasing the value of non-dimensional visco-damping coefficient.
- The wave propagation of TA type delays by increasing non-dimensional visco-damping coefficient.

Acknowledgements The work described in this paper was supported by National Natural Science Foundation of China (Grant no. 11972204). The authors are grateful for their supports.

References

1. He F, Luo Z, Li L, Zhang Y, Guo S (2021) Structural similitudes for the vibration characteristics of concave thin-walled conical shell. *Thin-Walled Struct* 159:107218. <https://doi.org/10.1016/j.tws.2020.107218>
2. Fattahi AM, Safaei B, Qin Z, Chu F (2021) Experimental studies on elastic properties of high density polyethylene-multi walled carbon nanotube nanocomposites. *Steel Compos Struct* 38:187. <https://doi.org/10.12989/scs.2021.38.2.177>
3. Fan F, Safaei B, Sahmani S (2021) Buckling and postbuckling response of nonlocal strain gradient porous functionally graded micro/nano-plates via NURBS-based isogeometric analysis. *Thin-Walled Struct* 159:107231. <https://doi.org/10.1016/j.tws.2020.107231>
4. Fan F, Sahmani S, Safaei B (2021) Isogeometric nonlinear oscillations of nonlocal strain gradient PFGM micro/nano-plates via NURBS-based formulation. *Compos Struct* 255:112969. <https://doi.org/10.1016/j.compstruct.2020.112969>
5. Asmael M, Safaei B, Zeeshan Q, Zargar O, Nuhu AA (2021) Ultrasonic machining of carbon fiber–reinforced plastic composites: a review. *Int J Adv Manuf Technol*. <https://doi.org/10.1007/s00170-021-06722-2>
6. Qiu Y, Luo Z, Ge X, Zhu Y, Gao Y (2020) Impact analysis of the multi-harmonic input splicing way based on the data-driven model. *Int J Dyn Control* 8:1181–1188. <https://doi.org/10.1007/s40435-020-00700-4>
7. Karimzadeh S, Safaei B, Jen TC (2021) Predicting phonon scattering and tunable thermal conductivity of 3D pillared graphene and boron nitride heterostructure. *Int J Heat Mass Transf* 172:121145. <https://doi.org/10.1016/j.ijheatmasstransfer.2021.121145>
8. Sahmani S, Safaei B (2021) Large-amplitude oscillations of composite conical nanoshells with in-plane heterogeneity including surface stress effect. *Appl Math Model* 89:1792–1813. <https://doi.org/10.1016/j.apm.2020.08.039>
9. Alhijazi M, Zeeshan Q, Qin Z, Safaei B, Asmael M (2020) Finite element analysis of natural fibers composites: a review. *Nanotechnol Rev* 9:853–875. <https://doi.org/10.1515/ntrev-2020-0069>
10. Moradi-Dastjerdi R, Behdinan K, Safaei B, Qin Z (2020) Buckling behavior of porous CNT-reinforced plates integrated between active piezoelectric layers. *Eng Struct* 222:111141. <https://doi.org/10.1016/j.engstruct.2020.111141>
11. Moradi-Dastjerdi R, Behdinan K (2021) Stress waves in thick porous graphene-reinforced cylinders under thermal gradient environments. *Aerosp Sci Technol*. <https://doi.org/10.1016/j.ast.2020.106476>
12. Qiu Y, Zhu Y, Luo Z, Gao Y, Li Y (2021) The analysis and design of nonlinear vibration isolators under both displacement and force excitations. *Arch Appl Mech*. <https://doi.org/10.1007/s00419-020-01875-0>
13. Safaei B (2020) The effect of embedding a porous core on the free vibration behavior of laminated composite plates. *Steel Compos Struct* 35:659–670. <https://doi.org/10.12989/scs.2020.35.5.659>
14. Moradi-Dastjerdi R, Behdinan K (2021) Layer arrangement impact on the electromechanical performance of a five-layer multifunctional smart sandwich plate. In: *Advanced multifunctional lightweight aerostructures: design, development, and implementation*, Wiley, pp 1–24. <https://doi.org/10.1002/9781119756743.ch1>
15. Moradi-Dastjerdi R, Behdinan K (2021) Free vibration response of smart sandwich plates with porous CNT-reinforced and piezoelectric layers. *Appl Math Model*. <https://doi.org/10.1016/j.apm.2021.03.013>
16. Moradi-Dastjerdi R, Behdinan K (2020) Thermo-electro-mechanical behavior of an advanced smart lightweight sandwich plate. *Aerosp Sci Technol* 106:106142. <https://doi.org/10.1016/j.ast.2020.106142>
17. Zenkour AM, Sobhy M (2015) A simplified shear and normal deformations nonlocal theory for bending of nanobeams in thermal environment. *Phys E Low-Dimens Syst Nanostruct* 70:121–128. <https://doi.org/10.1016/j.physe.2015.02.022>
18. Safaei B, Moradi-Dastjerdi R, Behdinan K, Qin Z, Chu F (2019) Thermoelastic behavior of sandwich plates with porous polymeric core and CNT clusters/polymer nanocomposite layers. *Compos Struct*. <https://doi.org/10.1016/j.compstruct.2019.111209>
19. Sahmani S, Safaei B (2019) Nonlinear free vibrations of bi-directional functionally graded micro/nano-beams including nonlocal stress and microstructural strain gradient size effects. *Thin-Walled Struct* 140:342–356. <https://doi.org/10.1016/j.tws.2019.03.045>
20. Safaei B, Naseradinmousavi P, Rahmani A (2016) Development of an accurate molecular mechanics model for buckling behavior of multi-walled carbon nanotubes under axial compression. *J Mol Graph Model*. <https://doi.org/10.1016/j.jmkgm.2016.02.001>
21. Sahmani S, Safaei B (2019) Nonlinear free vibrations of bi-directional functionally graded micro/nano-beams including nonlocal stress and microstructural strain gradient size effects. *Thin-Walled Struct*. <https://doi.org/10.1016/j.tws.2019.03.045>
22. Karimiasl M, Ebrahimi F, Mahesh V (2020) On nonlinear vibration of sandwiched polymer—CNT/GPL—fiber nanocomposite nanoshells. *Thin-Walled Struct* 146:106431. <https://doi.org/10.1016/j.tws.2019.106431>
23. Tang H, Li L, Hu Y, Meng W, Duan K (2019) Vibration of nonlocal strain gradient beams incorporating Poisson's ratio and thickness effects. *Thin-Walled Struct* 137:377–391. <https://doi.org/10.1016/j.tws.2019.01.027>
24. Safaei B, Ahmed NA, Fattahi AM (2019) Free vibration analysis of polyethylene/CNT plates. *Eur Phys J Plus*. <https://doi.org/10.1140/epjp/i2019-12650-x>
25. Qin Z, Zhao S, Pang X, Safaei B, Chu F (2019) A unified solution for vibration analysis of laminated functionally graded shallow shells reinforced by graphene with general boundary conditions. *Int J Mech Sci*. <https://doi.org/10.1016/j.ijmeosci.2019.105341>
26. Karami B, Shahsavari D, Janghorban M, Li L (2018) Wave dispersion of mounted graphene with initial stress. *Thin-Walled Struct* 122:102–111. <https://doi.org/10.1016/j.tws.2017.10.004>
27. Karami B, Shahsavari D, Li L (2018) Hygrothermal wave propagation in viscoelastic graphene under in-plane magnetic field based on nonlocal strain gradient theory. *Phys E Low-Dimens Syst Nanostruct* 97:317–327. <https://doi.org/10.1016/j.physe.2017.11.020>
28. Bakhtiari M, Tarkashvand A, Daneshjou K (2020) Plane-strain wave propagation of an impulse-excited fluid-filled functionally graded cylinder containing an internally clamped shell. *Thin-Walled Struct* 149:106482. <https://doi.org/10.1016/j.tws.2019.106482>

29. Abad F, Rouzegar J (2019) Exact wave propagation analysis of moderately thick Levy-type plate with piezoelectric layers using spectral element method. *Thin-Walled Struct* 141:319–331. <https://doi.org/10.1016/j.tws.2019.04.007>
30. Safaei B, Moradi-Dastjerdi R, Qin Z, Behdinin K, Chu F (2019) Determination of thermoelastic stress wave propagation in nanocomposite sandwich plates reinforced by clusters of carbon nanotubes. *J Sandw Struct Mater*. <https://doi.org/10.1177/1099636219848282>
31. Mindlin R, Tiersten H (1962) Effects of couple-stresses in linear elasticity. *Arch Ration Mech Anal* 11:415–448
32. Eringen AC (1972) Nonlocal polar elastic continua. *Int J Eng Sci* 10:1–16. [https://doi.org/10.1016/0020-7225\(72\)90070-5](https://doi.org/10.1016/0020-7225(72)90070-5)
33. Eringen AC (2002) Nonlocal continuum field theories. In: *Nonlocal continuum field theories*, Springer Science & Business Media, pp 1–14. https://doi.org/10.1007/978-0-387-22643-9_1
34. Yang F, Chong ACM, Lam DCC, Tong P (2002) Couple stress based strain gradient theory for elasticity. *Int J Solids Struct* 39:2731–2743. [https://doi.org/10.1016/S0020-7683\(02\)00152-X](https://doi.org/10.1016/S0020-7683(02)00152-X)
35. Lam DCC, Yang F, Chong ACM, Wang J, Tong P (2003) Experiments and theory in strain gradient elasticity. *J Mech Phys Solids* 51:1477–1508. [https://doi.org/10.1016/S0022-5096\(03\)00053-X](https://doi.org/10.1016/S0022-5096(03)00053-X)
36. Fan F, Xu Y, Sahmani S, Safaei B (2020) Modified couple stress-based geometrically nonlinear oscillations of porous functionally graded microplates using NURBS-based isogeometric approach. *Comput Methods Appl Mech Eng* 372:113400. <https://doi.org/10.1016/j.cma.2020.113400>
37. Ebrahimi F, Barati MR (2018) Nonlocal strain gradient theory for damping vibration analysis of viscoelastic inhomogeneous nanoscale beams embedded in visco-Pasternak foundation. *J Vib Control* 24:2080–2095. <https://doi.org/10.1177/1077546316678511>
38. Yang Y, Wang J, Yu Y (2018) Wave propagation in fluid-filled single-walled carbon nanotube based on the nonlocal strain gradient theory. *Acta Mech Solida Sin* 31:484–492. <https://doi.org/10.1007/s10338-018-0035-5>
39. Yang X, Sahmani S, Safaei B (2020) Postbuckling analysis of hydrostatic pressurized FGM microsized shells including strain gradient and stress-driven nonlocal effects. *Eng Comput*. <https://doi.org/10.1007/s00366-019-00901-2>
40. Xie B, Sahmani S, Safaei B, Xu B (2020) Nonlinear secondary resonance of FG porous silicon nanobeams under periodic hard excitations based on surface elasticity theory. *Eng Comput*. <https://doi.org/10.1007/s00366-019-00931-w>
41. Ebrahimi F, Habibi M, Safarpour H (2019) On modeling of wave propagation in a thermally affected GNP-reinforced imperfect nanocomposite shell. *Eng Comput* 35:1375–1389. <https://doi.org/10.1007/s00366-018-0669-4>
42. Al-Furjan MSH, Oyarhossein MA, Habibi M, Safarpour H, Jung DW (2020) Wave propagation simulation in an electrically open shell reinforced with multi-phase nanocomposites. *Eng Comput* 1:3. <https://doi.org/10.1007/s00366-020-01167-9>
43. Zenkour AM, Sobhy M (2021) Axial magnetic field effect on wave propagation in bi-layer FG graphene platelet-reinforced nanobeams. *Eng Comput* 1:3. <https://doi.org/10.1007/s00366-020-01224-3>
44. Kocatürk T, Akbaş ŞD (2013) Wave propagation in a microbeam based on the modified couple stress theory. *Struct Eng Mech* 46:417–431. <https://doi.org/10.12989/sem.2013.46.3.417>
45. Lim CW, Zhang G, Reddy JN (2015) A higher-order nonlocal elasticity and strain gradient theory and its applications in wave propagation. *J Mech Phys Solids* 78:298–313. <https://doi.org/10.1016/j.jmps.2015.02.001>
46. Li L, Hu Y, Ling L (2015) Flexural wave propagation in small-scaled functionally graded beams via a nonlocal strain gradient theory. *Compos Struct* 133:1079–1092. <https://doi.org/10.1016/j.compstruct.2015.08.014>
47. Ma LH, Ke LL, Wang YZ, Wang YS (2017) Wave propagation in magneto-electro-elastic nanobeams via two nonlocal beam models. *Phys E Low-Dimens Syst Nanostruct* 86:253–261. <https://doi.org/10.1016/j.physe.2016.10.036>
48. Arefi M, Zenkour AM (2017) Analysis of wave propagation in a functionally graded nanobeam resting on visco-Pasternak's foundation. *Theor Appl Mech Lett* 7:145–151. <https://doi.org/10.1016/j.taml.2017.05.003>
49. Barati MR, Zenkour A (2017) A general bi-Helmholtz nonlocal strain-gradient elasticity for wave propagation in nanoporous graded double-nanobeam systems on elastic substrate. *Compos Struct* 168:885–892. <https://doi.org/10.1016/j.compstruct.2017.02.090>
50. Narendar S, Gopalakrishnan S (2011) Nonlocal wave propagation in rotating nanotube. *Results Phys* 1:17–25. <https://doi.org/10.1016/j.rinp.2011.06.002>
51. Sobhy M, Zenkour AM (2020) The modified couple stress model for bending of normal deformable viscoelastic nanobeams resting on visco-Pasternak foundations. *Mech Adv Mater Struct* 27:525–538. <https://doi.org/10.1080/15376494.2018.1482579>
52. Zenkour AM, El-Shahrany HD (2020) Hygrothermal effect on vibration of magnetostrictive viscoelastic sandwich plates supported by Pasternak's foundations. *Thin-Walled Struct* 157:107007. <https://doi.org/10.1016/j.tws.2020.107007>
53. Zenkour AM, El-Shahrany HD (2020) Vibration suppression of magnetostrictive laminated beams resting on viscoelastic foundation. *Appl Math Mech* 41:1269–1286. <https://doi.org/10.1007/s10483-020-2635-7>
54. Ebrahimi F, Haghi P (2017) Wave propagation analysis of rotating thermoelastically-actuated nanobeams based on nonlocal strain gradient theory. *Acta Mech Solida Sin* 30:647–657. <https://doi.org/10.1016/j.camss.2017.09.007>
55. Zeighampour H, Beni YT (2017) Size dependent analysis of wave propagation in functionally graded composite cylindrical microshell reinforced by carbon nanotube. *Compos Struct* 179:124–131. <https://doi.org/10.1016/j.compstruct.2017.07.071>
56. Ebrahimi F, Dabbagh A (2017) Wave propagation analysis of embedded nanoplates based on a nonlocal strain gradient-based surface piezoelectricity theory. *Eur Phys J Plus* 132:1–14. <https://doi.org/10.1140/EPJP/I2017-11694-2>
57. Shahsavari D, Karami B, Li L (2018) A high-order gradient model for wave propagation analysis of porous FG nanoplates. *Steel Compos Struct* 29:53–66. <https://doi.org/10.12989/scs.2018.29.1.053>
58. Barati MR (2018) Temperature and porosity effects on wave propagation in nanobeams using bi-Helmholtz nonlocal strain-gradient elasticity. *Eur Phys J Plus* 133:170. <https://doi.org/10.1140/EPJP/I2018-11993-0>
59. Liu H, Lv Z (2018) Uncertain material properties on wave dispersion behaviors of smart magneto-electro-elastic nanobeams. *Compos Struct* 202:615–624. <https://doi.org/10.1016/j.compstruct.2018.03.024>
60. Amiri A, Talebitooti R, Li L (2018) Wave propagation in viscous-fluid-conveying piezoelectric nanotubes considering surface stress effects and Knudsen number based on nonlocal strain gradient theory. *Eur Phys J Plus* 133:1–17. <https://doi.org/10.1140/EPJP/I2018-12077-Y>
61. Ma LH, Ke LL, Wang YZ, Wang YS (2018) Wave propagation analysis of piezoelectric nanoplates based on the nonlocal theory. *Int J Struct Stab Dyn*. <https://doi.org/10.1142/S0219455418500608>
62. Karami B, Shahsavari D, Li L (2018) Temperature-dependent flexural wave propagation in nanoplate-type porous heterogeneous material subjected to in-plane magnetic field. *J Therm Stress* 41:483–499. <https://doi.org/10.1080/01495739.2017.1393781>

63. She GL, Yuan FG, Ren YR (2018) On wave propagation of porous nanotubes. *Int J Eng Sci* 130:62–74. <https://doi.org/10.1016/j.ijengsci.2018.05.002>
64. She G-L, Yan K-M, Zhang Y-L, Liu H-B, Ren Y-R (2018) Wave propagation of functionally graded porous nanobeams based on non-local strain gradient theory. *Eur Phys J Plus* 133:1–9. <https://doi.org/10.1140/EPJP/I2018-12196-5>
65. Zeighampour H, Tadi Beni Y, Botshekanan Dehkordi M (2018) Wave propagation in viscoelastic thin cylindrical nanoshell resting on a visco-Pasternak foundation based on nonlocal strain gradient theory. *Thin-Walled Struct* 122:378–386. <https://doi.org/10.1016/j.tws.2017.10.037>
66. Ebrahimi F, Dabbagh A (2019) Wave dispersion characteristics of heterogeneous nanoscale beams via a novel porosity-based homogenization scheme. *Eur Phys J Plus* 134:1–8. <https://doi.org/10.1140/EPJP/I2019-12510-9>
67. Masoumi A, Amiri A, Talebitooti R (2019) Flexoelectric effects on wave propagation responses of piezoelectric nanobeams via nonlocal strain gradient higher order beam model. *Mater Res Express* 6:1050d5. <https://doi.org/10.1088/2053-1591/ab421b>
68. Karami B, Janghorban M (2019) A new size-dependent shear deformation theory for wave propagation analysis of triclinic nanobeams. *Steel Compos Struct* 32:213–223. <https://doi.org/10.12989/scs.2019.32.2.213>
69. Wang YQ, Liang C (2019) Wave propagation characteristics in nanoporous metal foam nanobeams. *Results Phys* 12:287–297. <https://doi.org/10.1016/j.rinp.2018.11.080>
70. Sobhy M, Zenkour AM (2019) Wave propagation in magneto-porosity FG bi-layer nanoplates based on a novel quasi-3D refined plate theory. *Waves Random Complex Media*. <https://doi.org/10.1080/17455030.2019.1634853>
71. Abouelregal AE, Zenkour AM (2019) Vibration of FG viscoelastic nanobeams due to a periodic heat flux via fractional derivative model. *J Comput Appl Mech* 50:148–156. <https://doi.org/10.22059/jcamech.2019.277115.367>
72. Arani AG, Pourjamshidian M, Arefi M, Ghorbanpour Arani MR (2019) Application of nonlocal elasticity theory on the wave propagation of flexoelectric functionally graded (FG) timoshenko nano-beams considering surface effects and residual surface stress. *Smart Struct Syst* 23:141–153. <https://doi.org/10.12989/sss.2019.23.2.141>
73. Cao DY, Wang YQ (2020) Wave dispersion in viscoelastic lipid nanotubes conveying viscous protein solution. *Eur Phys J Plus* 135:1–14. <https://doi.org/10.1140/EPJP/S13360-019-00074-3>
74. Faroughi S, Rahmani A, Friswell MI (2020) On wave propagation in two-dimensional functionally graded porous rotating nanobeams using a general nonlocal higher-order beam model. *Appl Math Model* 80:169–190. <https://doi.org/10.1016/j.apm.2019.11.040>
75. Attia MA, Mahmoud FF (2016) Modeling and analysis of nanobeams based on nonlocal-couple stress elasticity and surface energy theories. *Int J Mech Sci* 105:126–134. <https://doi.org/10.1016/j.ijmecsci.2015.11.002>
76. Sourki R, Hosseini SA (2017) Coupling effects of nonlocal and modified couple stress theories incorporating surface energy on analytical transverse vibration of a weakened nanobeam. *Eur Phys J Plus* 132:1–14. <https://doi.org/10.1140/epjp/i2017-11458-0>
77. Ebrahimi F, Barati MR (2018) Stability analysis of porous multi-phase nanocrystalline nonlocal beams based on a general higher-order couple-stress beam model. *Struct Eng Mech* 65:465–476. <https://doi.org/10.12989/sem.2018.65.4.465>
78. Abouelregal AE, Mohammed WW (2020) Effects of nonlocal thermoelasticity on nanoscale beams based on couple stress theory. *Math Methods Appl Sci*. <https://doi.org/10.1002/mma.6764>
79. Ebrahimi F, Barati MR (2018) A modified nonlocal couple stress-based beam model for vibration analysis of higher-order FG nanobeams. *Mech Adv Mater Struct* 25:1121–1132. <https://doi.org/10.1080/15376494.2017.1365979>
80. Shariati A, Barati MR, Ebrahimi F, Toghroli A (2020) Investigation of microstructure and surface effects on vibrational characteristics of nanobeams based on nonlocal couple stress theory. *Adv Nano Res* 8:191–202. <https://doi.org/10.12989/anr.2020.8.3.191>
81. Ramezani SR, Mojra A (2020) Stability analysis of conveying-nanofluid CNT under magnetic field based on nonlocal couple stress theory and fluid-structure interaction. *Mech Based Des Struct Mach*. <https://doi.org/10.1080/15397734.2020.1851254>
82. Attar F, Khordad R, Zarifi A, Modabberasl A (2021) Application of nonlocal modified couple stress to study of functionally graded piezoelectric plates. *Phys B Condens Matter* 600:412623. <https://doi.org/10.1016/j.physb.2020.412623>
83. Reddy JN (2007) Nonlocal theories for bending, buckling and vibration of beams. *Int J Eng Sci* 45:288–307. <https://doi.org/10.1016/j.ijengsci.2007.04.004>
84. Ebrahimi F, Barati MR, Haghi P (2018) Wave propagation analysis of size-dependent rotating inhomogeneous nanobeams based on nonlocal elasticity theory. *J Vib Control* 24:3809–3818. <https://doi.org/10.1177/1077546317711537>
85. Gopalakrishnan S, Narendar S (2013) Wave propagation in nanostructures: nonlocal continuum mechanics formulations. *Spring Sci Bus Media*. https://doi.org/10.1007/978-3-319-01032-8_3
86. Gopalakrishnan S (2016) Wave propagation in materials and structures. CRC Press
87. Eltahir MA, Khater ME, Emam SA (2016) A review on nonlocal elastic models for bending, buckling, vibrations, and wave propagation of nanoscale beams. *Appl Math Model* 40:4109–4128. <https://doi.org/10.1016/j.apm.2015.11.026>
88. Ebrahimi F, Dabbagh A (2019) Wave propagation analysis of smart nanostructures. CRC Press

Publisher's Note Springer Nature remains neutral with regard to jurisdictional claims in published maps and institutional affiliations.